Power Converters Control for Photovoltaic Water Pumping System

Bruno Henrique Boschetti Tangerino

Thesis Presented to the School of Technology and Management of Polytechnic Institute of Bragança to the Fulfilment of the Requirements for the Master of Science Degree in Industrial Engineering (Electrical Engineering branch).

Supervised by:

Professor Doutor Vicente Leite

Professor Doutor Alessandro Goedtel

Professora Doutora Ângela Ferreira

Bragança

2018

Power Converters Control for Photovoltaic Water Pumping System

Bruno Henrique Boschetti Tangerino

Thesis Presented to the School of Technology and Management of Polytechnic Institute of Bragança to the Fulfilment of the Requirements for the Master of Science Degree in Industrial Engineering (Electrical Engineering branch).

Supervised by:

Professor Doutor Vicente Leite

Professor Doutor Alessandro Goedtel

Professora Doutora Ângela Ferreira

Bragança

2018

Dedication

to Natalia,

my eternal love

Acknowledgment

First of all, to God, for all these years of strength and courage to face every challenge of life.

To my parents, Edson and Marcia, that are my foundation and supported me unconditionally since my first step.

To Natalia, love of my life, for her unconditional love and support.

To the Federal Technological University of Paraná (UTFPR) that guided me in the build of my character, in personal and professional way. I want to thank Professor Alessandro Goedtel for years of competent orientation and guideness. Thanks for Professor Murilo Silva, for his trust and help. Special thanks to my friends in CIPECA - LSI: Wagner Godoy, Rodrigo Palácios, Clayton Graciola, Tiago Drummond, Murillo Gentil, Igor Elias, Gustavo Bazan, Fabiano Carvalho, Gustavo Barbara and Enrique Santos.

To the Polytechnic Institute of Bragança (IPB), that accepted me to expand my horizon of knowledge. Thanks to Professor Vincente Leite, who is a exceptional professional and professor, for such dedication and orientation. I want to thank Professor Ângela Ferreira and Professor José Batista for excellent orientation and support. Special thanks to my laboratory friends Paulo Araújo and Alison Nakashima.

To three exceptional people: Matheus Montanini Breve, for all the helping and support; Wellington Maidana Silva, a true brother; and Dionízio José Vargas Roman, for all the work together.

Finally, I want to thank every single person who directly or indirectly was part of my trajectory through the graduation and master's degree and making memorable these years of studying.

Abstract

This work proposes solutions to challenges encountered in photovoltaic water pumping systems, such as the issue in the number of photovoltaic modules in low power systems, the maximum power point tracking and its implementation, as well as the pump control system. The maximum power point tracking is achieved via the addition of a step-up converter controlled by a proportional-integral controller. The system load is comprised by an induction motor, controlled by an open-loop scalar strategy. Simulations and real platform tests with solar radiance variation and variable number of photovoltaic modules were performed, validating the operation of the proposed solutions.

Keywords: Photovoltaic Water Pumping System; Maximum Power Point Tracking; Open-Loop Scalar Control; Control Methods; Induction Motor.

Resumo

Este trabalho propõe soluções para os desafios encontrados nos sistemas de bombagem fotovoltaica, como a questão do número de módulos fotovoltaicos em sistemas de baixa potência, o seguimento do ponto de potência máxima e sua implementação, bem como o sistema de controle da bomba. O seguimento do ponto de potência máximo é obtido através da adição de um conversor elevador, controlado por um controlador proporcional-integral. A carga do sistema é compreendida por um motor de indução, controlado por uma estratégia de controle escalar em malha aberta. Simulações e testes em uma plataforma real, com variação do nível de radiação solar e um número variável de módulos fotovoltaicos foram realizados, validando o funcionamento das soluções propostas.

Palavras-chave: Sistema de Bombagem Fotovoltaica de Água; Reatreamento do Ponto de Potência Máxima; Controle Escalar em Malha Aberta; Motor de Indução.

Contents

List of Tables

List of Figures

Nomenclature

Abbreviations

AC	Alternating Current
DC	Direct Current
IGBT	Insulated Gate Bipolar Transistor
MPP	Maximum Power Point
MPPT	Maximum Power Point Tracking
NOCT	Normal Operating Cell Temperature
P&O	Perturb and Observe method
PI	Proportional-Integral
PID	Proportional-Integral-Derivative
PV	Photovoltaic
PVWPS	Photovoltaic Water Pumping System
PWM	Pulse-Width Modulation
SS	Steady-state
SFC	Standard Frequency Converter

STC Standard Test Conditions

Symbols

C	Capacitance
D	Duty cycle
E_l	Induced electromotive force
$E(s)$	System response error
η	Efficiency
f	Frequency
f_s	Switching frequency
G	Solar radiation level
i_C	Capacitor current
i_L	Inductor current
I_{ph}	Photovoltaic current of the photovoltaic cell
I_{pm}	Maximum power current
I_{pv}	Current sensed from the PV panel
I_{SC}	Short-circuit current under STC
K_h	Constant of motor construction
K_i	Integral gain
K_p	Proportional gain

L	Inductance
L_{min}	Minimum inductance
N	Number of turns per phase in the stator
P	Power
R_s	Stator resistance
R	Resistance
R_L	Load resistance
T	Period
t	Time
T_a	Ambient temperature
T_i	Integrative time
V_{boost}	Offset voltage
V_L	Inductor voltage
V_m	Motor voltage
V_O	Output voltage
V_{OC}	Open-circuit voltage under STC
V_{ph}	Supply-phase voltage
V_{pm}	Maximum power voltage
V_{pv}	Voltage sensed from the PV panel
V_{SP}	Setpoint voltage

Chapter 1

Introduction

In 2010, studies showed that over 900 million people in various countries do not have water for consumption [1]. This occurs by the difficulty on the access of this resource, because a large amount of these people are isolated, located on rural areas, where the water supply comes from rain or distant rivers [2]. These regions do not have access to the national grid system to pump water for irrigation purpose in farming and consumption. As an example, the lack of electricity is one of the main hurdles in the development in rural India, where electrical and diesel-powered water pumping systems are widely used for the applications cited [3], [4].

Moreover, environmental issues and impacts such population and global warming effects have created the interest in fossil fuels usage reduction and development in renewable energy resources. Water pumping systems, using different forms of energies, have been proposed as a solution for water supply. Solar-thermal, wind energy and hybrid systems are the most investigated forms of energy for this purpose [5].

One of the most efficient and promising way to solve the water catchment problem in isolated areas is the use of solar powered systems, supplied by photovoltaic (PV) solar energy. This type of energy source is becoming cheaper and has already been put to work for several years in various countries around the world [1].

The PV pumping had great progress since its first application in the 1970's. Its expansion occurs through the reduction of the price of its components, the technological

improvement, the governmental initiative and through programs of International Cooperation [6]. Studies showed that solar energy is growing interest and offers a satisfactory solution to supply desert and isolated regions, as one of the most typical applications in developing countries and has a potential to become a major force for social and economic development [7].

1.1 Objectives

The objective of this work is to develop a photovoltaic water pumping system control for the power structures of the pumping system, such as the maximum power point tracking and the scalar control of the induction motor.

Control dynamics and load response (induction motor) must match in order to obtain the proper operation of the system. To achieve this, it is intended to develop a PI controller for the step-up converter to extract the maximum power available from the PV generation and an open-loop strategy to control the motor.

1.2 Plan of Thesis

The present document is constituted by seven chapters. After the introduction, the state of the art presents a brief description of the system, along with a solar photovoltaic energy panorama and the explanation of the components that compose and control the PV water pumping system.

On the third chapter, the control methods utilized on the system, for maximum power point tracking and control of the induction machine, are presented.

On the fourth and fifth chapters, simulations results of the step-up converter and the single-phase induction motor and experimental evaluation and validation of the proposed solutions are presented, respectively.

Lastly, conclusions of the work are presented along with the future works developments prospects.

Chapter 2

State of the Art

Currently, solar systems are used to pump water in various regions around the world [8]. With the solar energy generation expansion, the development of solar powered technologies and the need of water pumping in many areas for consumption and irrigation are two significant factors that motivates and challenges researchers of various engineering fields to optimize, simplify and lower the cost of this kind of water pumping system.

This chapter presents the studies about the solar photovoltaic (PV) energy in water pumping systems and its components, showing its evolution, the functioning of every stage of the conversion of the solar energy to drive a single-phase standard pump and the approach to extract the maximum power for water pumping.

2.1 System Description

The system proposed for the photovoltaic water pumping on this work is constituted by five subsystems. Additionally, one control method for the generation, one for the load (water pump), and the measurement of voltages and currents along the entire system, to perform such controls. The electrical scheme is shown on Figure 2.1.

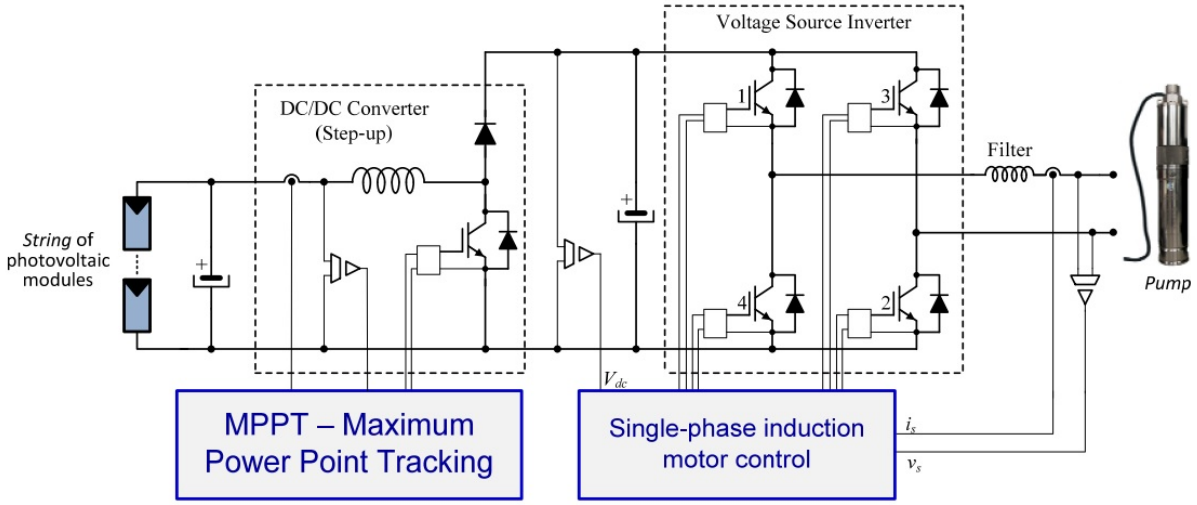

Figure 2.1: Electrical scheme of the photovoltaic water pumping System.

The subsystems are:

- Power Generation: string of photovoltaic modules that composes the solar power generation;
- Step-up Converter: a DC/DC converter that elevates the voltage from the generation for the inverter required values;
- DC-link: composed by a capacitor, is the source voltage of the inverter;
- Voltage Source Inverter: converts the DC-link to an AC voltage source to drive the motor of the pump;
- Pump: a single-phase induction motor with a turbine;
- MPPT: algorithm that defines the operation point of the generation to extract the maximum power on specific conditions;
- Open-Loop Scalar Control: a control method for induction machines, mostly speed control.

On the next sections, each subsystem will be explained, along with an overview of the solar photovoltaic energy.

2.2 Solar Photovoltaic Energy Panorama

The solar photovoltaic power capacity is growing around the world, due to its simple generation and competitive prices among others renewable energy sources, like wind. According to Solar Power Europe studies, the global market of PV energy in 2016 has grown over 50% compared with 2015 [9]. Europe itself had an increase of solar PV capacity installed from 91,7 GW to 103,8 GW (approximately 6.45%), being the first world region surpassing the 100 GW mark, and over 170 GW possible by 2020, as shown in Figure 2.2.

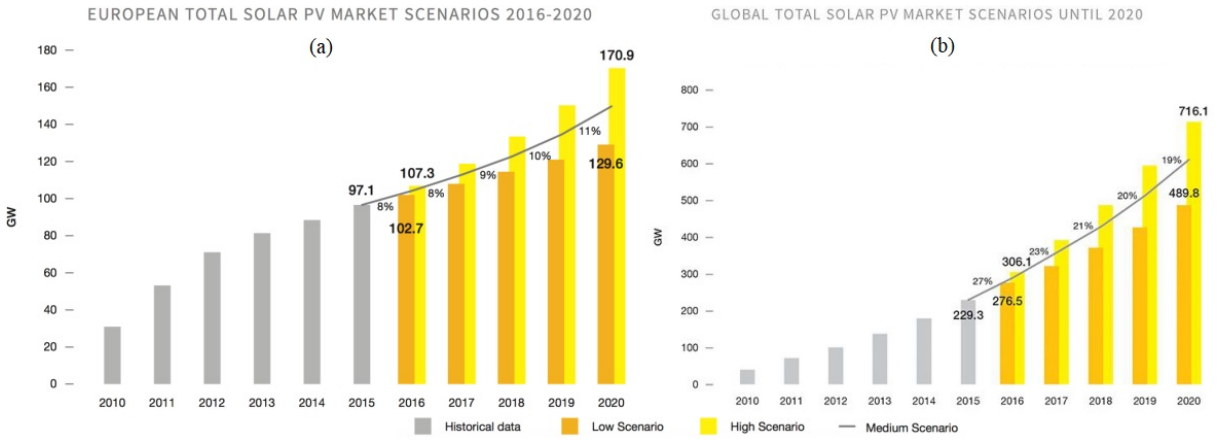

Figure 2.2: Total solar PV market scenarios - 2016/2020: (a) Europe. (b) World. Adapted from [10].

As observed in Table 2.1, the Europe's net power generation shows that solar PV energy is among the top 3 electricity sources, behind wind and gas [10]. With this data, it is easy to see the importance of solar PV energy and its evolution along the years.

Table 2.1: Europe's net power capacities added from 2000-2015.

Energy Sources	**Capacities added [GW]**
Wind	137.5
Gas	120.6
Solar	95.4
Others	25.51
Nuclear, Coal and Fuel Oil	-84 (Decommissioned)

2.3 Photovoltaic Water Pumping Systems

Nowadays, more than 900 million people in various countries do not have access to water for consumption, and a large parcel is found isolated from the national grid or areas where the water supply comes from the rain or near rivers. The difficulty of water access in these regions does not simply affect the consumption, but the irrigation systems also, among other usages [2]. The utilization of PV solar energy to power water pumps is a challenging technology that is being more and more utilized due to its advantages on this application and it also presents an environmentally favorable alternative to fossil fuel powered conventional water pumps. An important point to be highlighted is the enormously acceptance, reliability and performance gained by this type of system [11].

The advantages of using solar PV energy to pump water are various, which includes that solar photovoltaic water pumping systems (PVWPS) can withstand severe weather conditions and the existence of a natural relationship between requirement of water and availability of solar power. PVWPS are constituted by different components, which can be divided by electrical, electronic and mechanical components. Each one has its construction, values and working performance characteristics, making possible to attend needs of different users [11].

In contrast, these components need an acceptable level of integration and synchronization, otherwise poor performance in operation of the system may occur. But, involvement of sophisticated technology in the system requires technical expertise for its operation and maintenance. These factors motivated and challenged researchers of various fields of engineering to contribute and make SPVWPS more efficient, simple and cost-effective, and making this area of research hold a large scope in water pumping methods [11].

2.4 Solar Cell

Energy exists in different forms and can be converted from one to another. Solar energy can be converted to thermal, chemical or electrical energy depending on the kind

of interaction between solar radiation (photon) and matter. Photon-matter interaction in photovoltaic energy conversion route involves excitation of electrons to higher potential energy level (photovoltage generation) and subsequent separation of charge from its excited state to produce electricity. For this energy conversion, materials called semiconductors are used, due to its electrical and optical properties [12].

2.4.1 Model of a Solar Cell

A solar cell is considered as a current source as shown in Figure 2.3. Though the practical behaviour of a cell is deviated from ideal due to electrical and optical losses, yet in order to develop an electric equivalent circuit model for solar cells, appropriate components should be added with ideal current source (representing solar cell) [12].

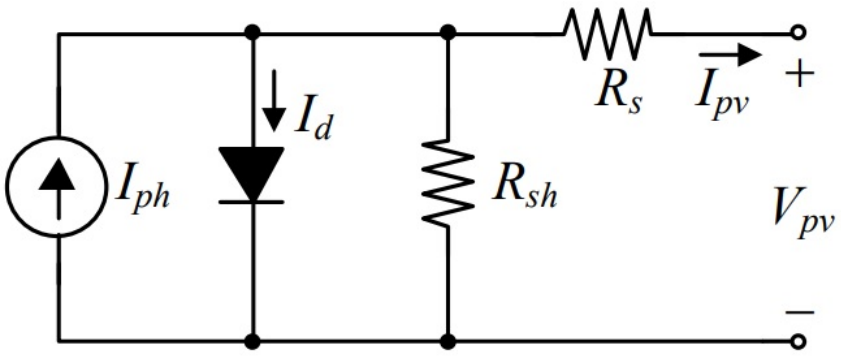

Figure 2.3: Solar cell electrical equivalent circuit model.

The optical loss is represented by the current source itself, where the generated current is proportional to the light input. The recombination losses are represented by the diode connected parallel to the circuit source, but in the reverse direction (as the recombination current flows in the opposite direction to the light-generated current). The ohmic losses in the cell occur due to series and shunt resistances denoted by R_S and R_{sh}, respectively. The series resistance, as the name suggests, is the resistance offered by the solar cell in the path of current flow. The shunt resistance is referred as the leakage path of the current in a solar cell [12].

The photovoltaic current of the PV cell (I_{ph}) is proportional to the solar radiation level falling on the cell [13]:

$$I_{ph} = [I_{SC} + K_f(T_c - T_r)]\frac{G}{G_r} \tag{2.1}$$

Where:

- I_{ph}: Photovoltaic current of the PV cell;
- I_{SC}: Short-circuit current under Standard Test Conditions (STC), $T_c = 25°C$ and G = 1000 W/m^2;
- K_f:Temperature factor of short circuit current (0,0017A/°C);
- T_c: PV cell temperature (in Kelvin);
- T_r: Reference temperature (298,15 K);
- G: Solar radiation level;
- G_r: Reference solar radiation level (1000 W/m^2).

Diode current (I_D), depends on the voltage and reverse leakage current (I_o)[13]:

$$I_D = I_o\left(e^{\frac{q.V_{pv}}{A.k.T_c}} - 1\right) \tag{2.2}$$

Where:

- q: Electron charge (1,602x10^{-19}C);
- k: Boltzman constant (1,3806505x10$^{-23}J/K$);
- A: Quality factor of diode.

The equation of the current flowing through the shunt resistance:

$$I_{sh} = \frac{V_D}{R_{sh}} = \frac{V_{pv} + I_{pv}R_S}{R_{sh}} \tag{2.3}$$

PV cell output voltage and current is given by[13]:

$$V_{pv} = V_D - I_{pv}R_S \tag{2.4}$$

$$I_{pv} = I_{ph} - I_D - I_{sh} \tag{2.5}$$

The following mathematical model is obtained when equations 2.2 and 2.3 are substituted in equation 2.5 [13]:

$$I_{pv} = I_{ph} - I_o \left[e^{\frac{q(V_{pv}+I_{pv}R_S)}{A.k.T_c}} - 1 \right] - \frac{V_{pv} + I_{pv}R_S}{R_{sh}} \tag{2.6}$$

These mathematical model and equations are important to analyze the behaviour of the solar module with variation of radiation and temperature. A PV module is a set of PV cells assembled in a framework. Typically, a PV module has 36 cells, 15 cm x 15 cm, connected in series.

2.4.2 Solar Cell Characteristics - Radiation and Temperature Variation

To analyze a PV system, we should look at the I-V and P-V curves of the PV module, that gives crucial information when it is put under application. Two principal parameters on the PV module are:

- Short-circuit current (I_{SC}): the maximum current that flows in a solar module when its terminals are shorted, i. e., $V_{pv} = 0$ V;
- Open-circuit voltage (V_{OC}): the maximum voltage generated across the terminals of the PV module when they are kept open, i. e., $I_{pv} = 0$ A.

Simulations were built on Matlab to ease the visualization of the I-V and P-V curves [14]. The PV module used was a Fluitecnik's FTS-220P model [15], which characteristics are shown in Table 2.2. There are available 9 of these modules on the roof of the

electromechanical systems laboratory, which can be configured in strings with different number of PV modules.

Table 2.2: PV Module FTS-220P electrical characteristics.

Electrical Characteristics	**Value**
P_{max} Maximum power	220 W
V_{pm} Maximum power voltage	29,38 V
I_{pm} Running at maximum power	7,51 A
V_{OC} Open-circuit voltage	36,76 V
I_{SC} Short-circuit current	8,30 A
NOCT Standard operating temperature	$46°C \pm 2°C$
T_{kP} Temperature coefficient of P_{max}	-0,45%/°C
T_{kI} Temperature coefficient of I_{SC}	+0,006%/°C
T_{kV} Temperature coefficient of V_{OC}	-0,33%/°C

As the current is proportional to radiation level, the current increases with higher indexes of solar radiation falling on the PV cell. On the other hand, the voltage varies a little [16]. The I-V and P-V curves for radiation variation are shown on Figure 2.4.

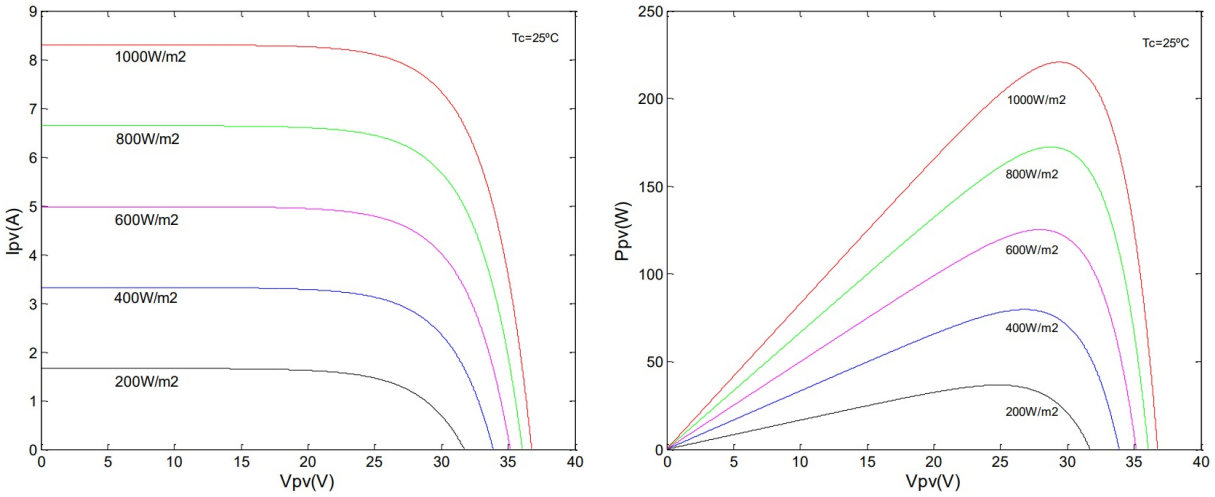

Figure 2.4: I-V and P-V curves for FTS-220P module under radiation variation [14].

With higher cell temperatures, the voltage of the PV cell suffers a significant decrease, while the maximum current varies a little. On the P-V curve, the maximum power varies

less with the variation of solar radiation, but the maximum power point varies considerably [16]. The I-V and P-V curves for temperature variation are shown on Figure 2.5.

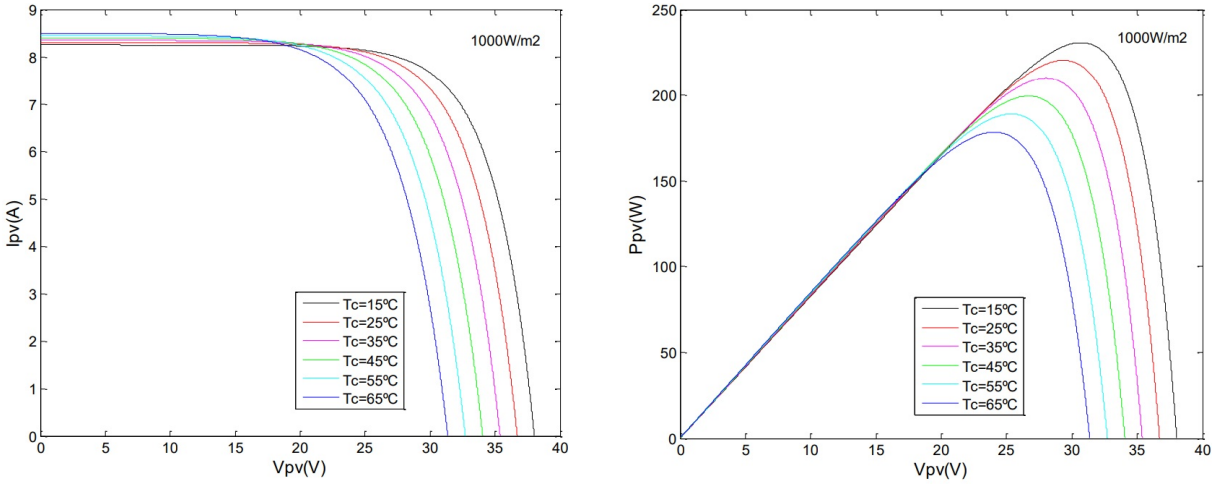

Figure 2.5: I-V and P-V curves for FTS-220P module under temperature variation [14].

Other parameter analyzed on PV system are the Maximum Power Point (MPP), which is the point where the PV system provides the maximum power. This subject will be explained on next section.

2.5 Maximum Power Point Tracking

Nowadays, PV generators are one of the most prominent ways to produce electrical energy over the world [10]. A general issue in PV energy generation is the tracking to extract the maximum power (MP) available at the PV array output. The need for an algorithm to follow the maximum power point (MPP) comes from the non-linearity of the I-V characteristic of a PV cell. The MPPT technique consists of adjusting the output voltage of the PV to extract the MP independent of changes in the radiation or temperature.

At the present time, around 40 listed MPPT methods are proposed in literature, and each one has its own specifications, limitations, applications, vantages and disadvantages [17].

Zamora et al. [18] did an efficiency based comparative analysis between three frequently used MPPT methods, which are Hill Climbing (HC), Perturb and Observe (P&O) and Incremental Conductance (INC). Their analysis is oriented to measure the efficiency of each algorithm, using the following criteria: ease of implementation, number of sensors utilized, efficiency, cost and type of application. The simulation results in steady-state are shown in Table 2.3.

Table 2.3: Comparison of MPPT Algorithms [18].

MPPT Algorithm	**Maximum time to track in steady-state**	**Minimum power loss in steady-state**	**Efficiency** η
HC	160 ms	1,7W	97,04%
P&O	166 ms	1,5W	97,26%
INC	188 ms	0,5W	98,00%

For this work, the MPPT method implemented is P&O algorithm, due to its simplicity and low computational resources [18]. P&O is the most common method of MPPT algorithms, due to that is widely used in the control system of the power converters in PV applications and is not required the information of solar panel characteristics to make the maximum power point tracking [19].

The P&O algorithm measures the voltage and current at the output of the PV array and the operating point is calculated (actual power point and voltage point) to perturb the voltage and make a comparison with a previous operating point (previous power point and voltage point), obtaining the slope value of dP/dV (Figure 2.6).

If dP/dV is greater than zero, it is known that the perturbation moved the array's operating point toward the MPP and the algorithm would then continue to perturb the PV array voltage in the same direction. On the other hand, if dP/dV is smaller than zero, then the change in operating point moved the PV array away from the MPP, and the P&O algorithm invert the direction of the voltage perturbation [20]. The steps followed by the algorithm are illustrated on the flow chart of the Figure 2.7 with the variables defined in the Table 2.4.

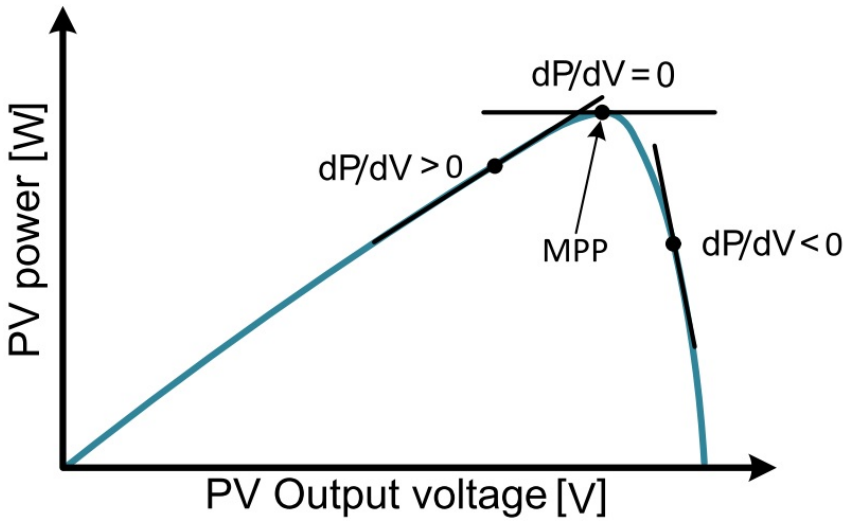

Figure 2.6: PV curve slope (adapted from [18]).

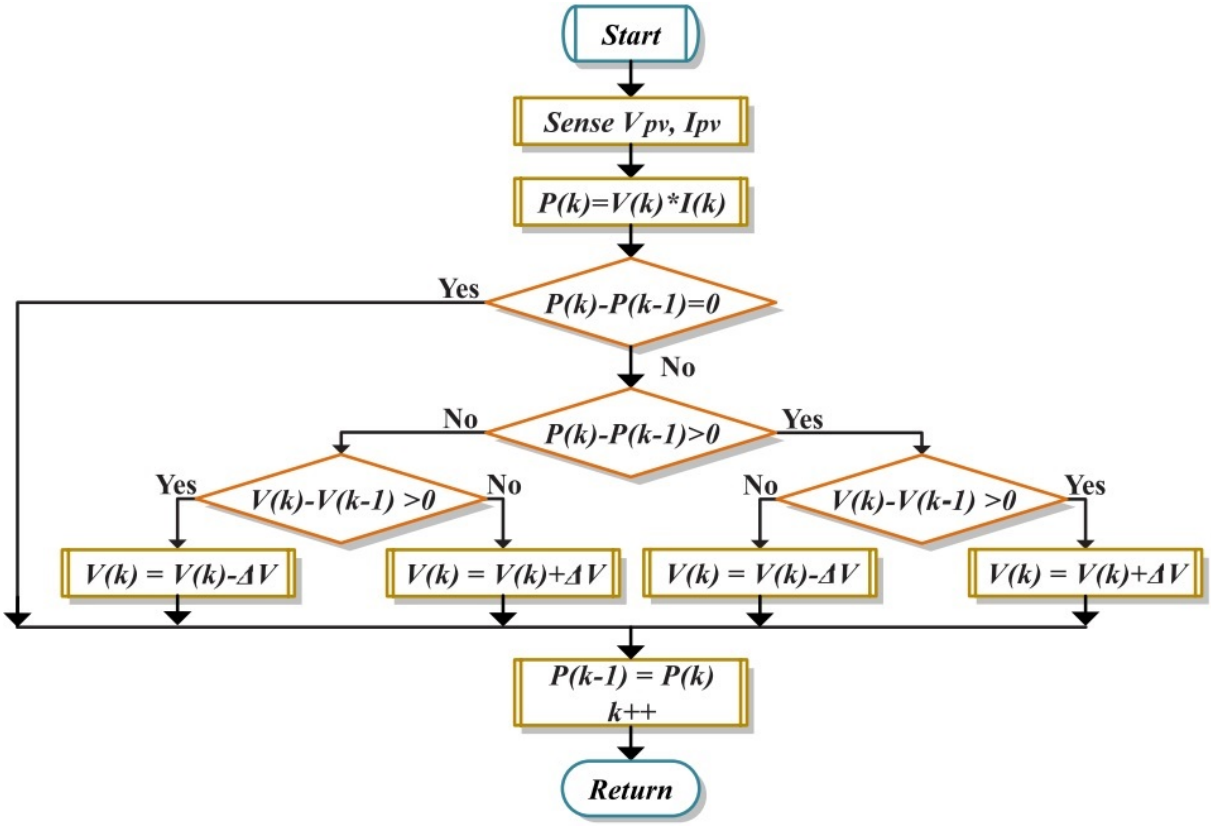

Figure 2.7: State flow chart of P&O MPPT algorithm [18].

Table 2.4: Description of variables presented in flow chart [18].

Variable	**Description**
V_{pv}	Voltage sensed from the PV Panel
I_{pv}	Current sensed from the PV Panel
$P(k)$, $V(k)$, $I(k)$	Power, Voltage and Current in present iteration
$P(k-1)$, $V(k-1)$, $I(k-1)$	Power, Voltage and Current in past iteration
ΔV	Voltage increment
$k++$	Change for next iteration

2.6 Proportional-Integral Control

The operation of the PI controller is based on two values: the reference (set-point) and the actual value (measured). The difference between the reference and the actual value is the error signal which is applied to the input of the PI controller, which actuates on the control variable, adjusting it to control the system.

An increase in proportional gain (K_p) value of the proportional term will accelerate the system response and reduce the effects of disturbances and sensibility of parameters variation of the system. Although, high values of K_p will lead to instability and errors amplifications. To overcome this situation, an integral term (K_i) is added to the controller. The main advantage of the integral term is to reduce or eliminate steady-state errors. Still, as the integral term (Equation 2.7) accumulates past errors, high values for K_i makes the system become less stable.

The Proportional-Integral control action is given by:

$$u(t) = K_p e(t) + K_i \int_0^t e(t)dt \tag{2.7}$$

applying Laplace transform:

$$G_{pi}(s) = \frac{U(s)}{E(s)} = K_p + \frac{K_i}{s} = K_p \left(1 + \frac{1}{T_i s}\right) \tag{2.8}$$

where $K_i = K_p/T_i$.

2.7 DC/DC Converters - Step-up

DC/DC converters are power electronic circuits for power processing that convert a DC voltage value to another level, higher or lower, depending on the converter. There are a lot of types of converters, and they are used in large scale in many areas, like uninterruptible power supplies, electrical drives, renewable systems, DC motor control systems and so on [21].

The basic DC/DC converter works with a switch and a DC voltage source. Assuming the switch is ideal (no losses), the output DC voltage is the same of the input when the switch is closed, and is zero when the switch is open. Periodic opening and closing of the switch results in a DC output voltage controlled by adjusting the duty ratio D, which is the fraction of the period that the switch is closed [21].

$$D \equiv \frac{t_{on}}{t_{on} + t_{off}} = \frac{t_{on}}{T} = t_{on} f \tag{2.9}$$

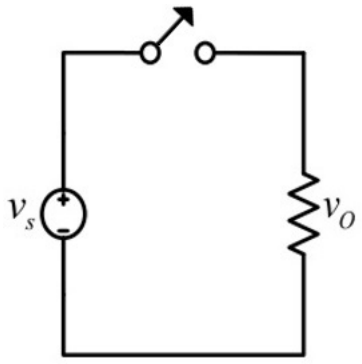

Figure 2.8: A basic DC/DC switching converter.

The output voltage V_O is defined by the ratio D. For example, Figure 2.8 shows a simple DC/DC converter that when the ratio D is equal to zero, the switch is always open and V_O is zero. If D is equal to one, the switch is always closed and $V_O = V_S$. Variating the ratio D between zero and one, the average output voltage, V_O, variates between 0 and

V_S [21].

The step-up converter is a switching circuit that elevates the value of the input voltage to the output [21]. This converter is formed by a diode, an inductor, a capacitor and a switch. Its configuration is shown on the Figure 2.9(a).

The analysis of this converter proceeds by examining the behavior of the inductor voltage and current for two distinct situations: switch open and switch closed. To analyze these values in these situations, it is assumed that the inductor current is continuous (always positive), the capacitor is very large and can maintain the output voltage V_O constant, and the components are ideal. The switching period is T, the switch closed time is DT and the switch open time is $(1 - D)T$ [21].

First Condition: in the closed switch time (DT), the diode is reverse biased. As shown in 2.9(b), the voltage in the inductor is equal to V_S, so

$$V_L = V_S = L\frac{di_L}{dt}$$

The variation in the current of the inductor is constant, so the current increases linearly when the switch is closed, as shown in Figure 2.10. This value is calculated from

$$\frac{\Delta i_L}{\Delta t} = \frac{\Delta i_L}{DT} = \frac{V_S}{L}$$

$$(i_L)_{closed} = \frac{V_S DT}{L} \tag{2.10}$$

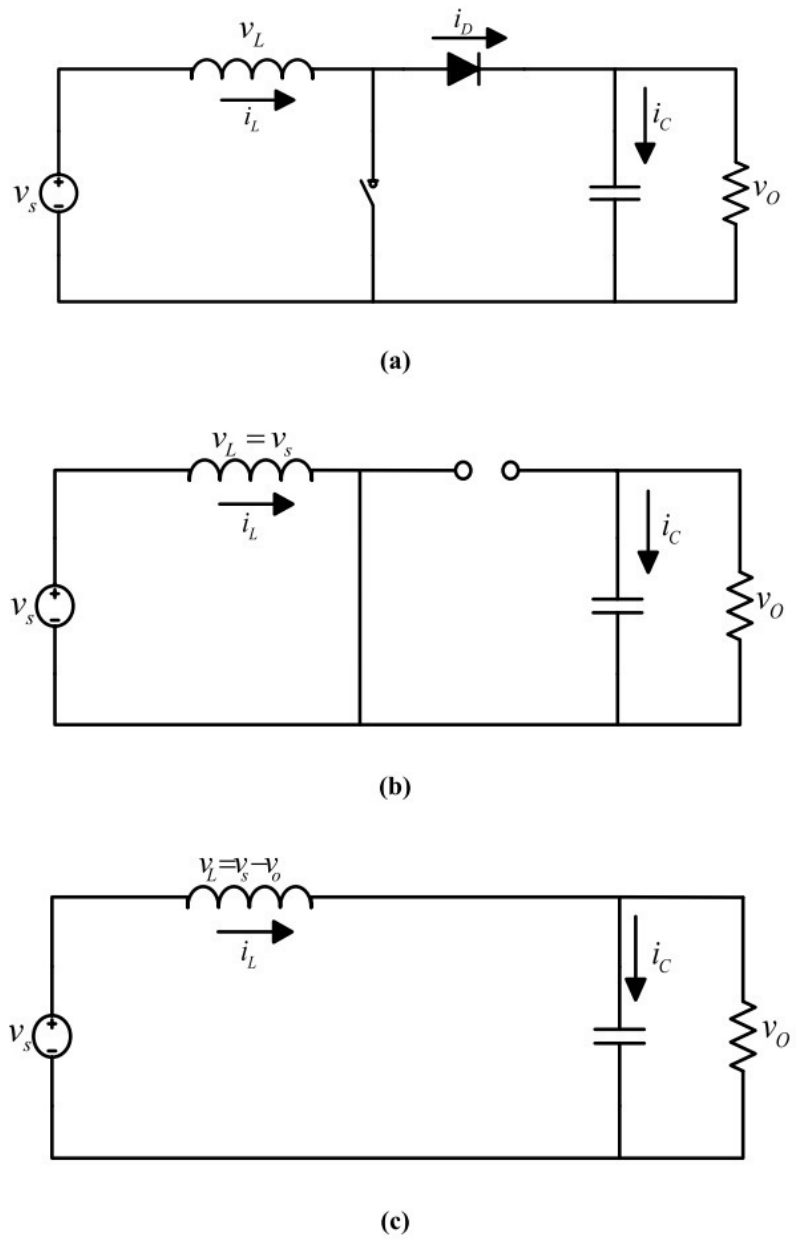

Figure 2.9: Step-up Converter: (a) circuit, (b) equivalent for the switch closed, (c) equivalent for the switch open, [21].

Second Condition: when the switch is open, the diode becomes forward biased, providing a path for the inductor current, as shown in Figure 2.9(c). Assuming that the output voltage V_O is constant, higher than V_s and knowing that the inductor current cannot change instantly [21], the voltage across the inductor is

$$V_L = V_S - V_O = L\frac{di_L}{dt}$$

$$\frac{di_L}{dt} = \frac{V_S - V_O}{L}$$

Again, the current change is constant and decreases linearly, since $V_L = V_S$ - V_O <0, while the switch is open, as shown in the Figure 2.11. The value of this variation is calculated by

$$\frac{di_L}{dt} = \frac{di_L}{(1-D)T} = \frac{V_S - V_O}{L}$$

solving for Δi_L,

$$(i_L)_{open} = \frac{(V_S - V_O)(1-D)T}{L} \tag{2.11}$$

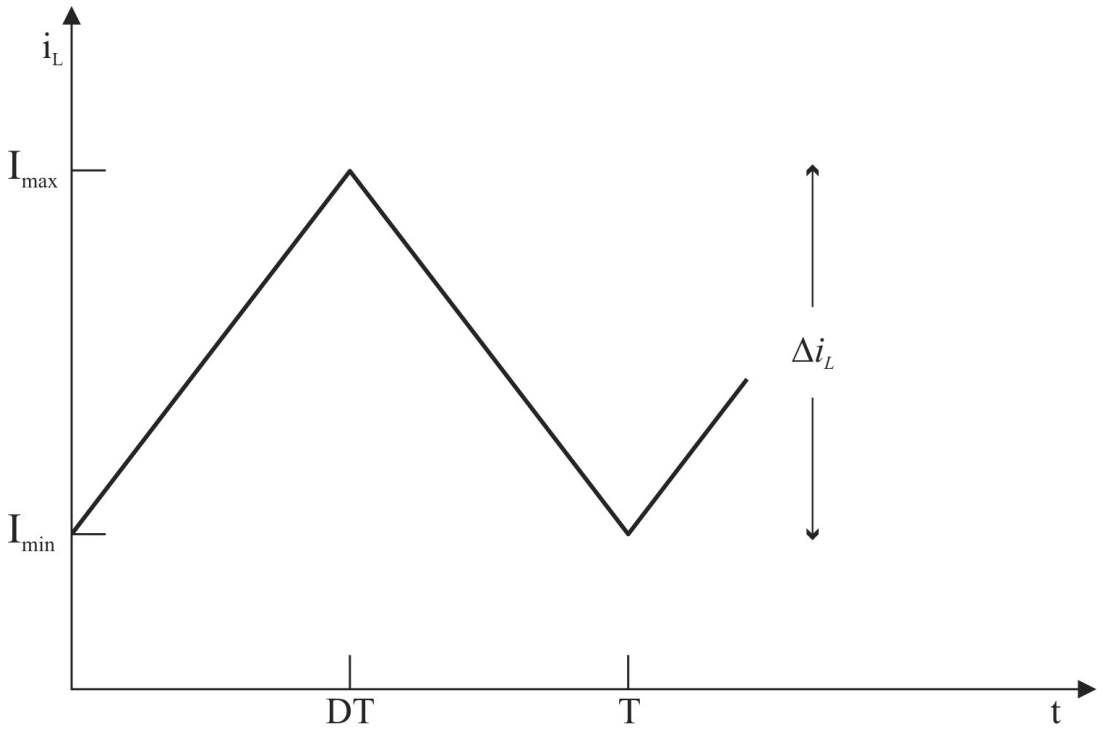

Figure 2.10: Inductor current waveform. [21]

For steady-state operation, the net change in the inductor must be zero [21]. Thus:

$$(i_L)_{closed} + (i_L)_{open} = 0$$
$$\frac{V_S DT}{L} + \frac{(V_S - V_O)(1-D)T}{L} = 0$$

solving for V_O,

$$V_O = \frac{V_S}{1-D} \tag{2.12}$$

Also, the average inductor voltage must be zero for periodic operations [21]. Thus:

$$V_L = V_S D + (V_S - V_O)(1-D) = 0$$

solving for V_O,

$$V_O = \frac{V_S}{1-D}$$

that compares to the Equation 2.12.

These equations show that if the switch is always open ($D = 0$), the value for the voltage on the output is the same of the input. As the D ratio increases, V_O becomes larger than the V_S, elevating the voltage level. But, as the D ratio approaches one, the output goes to infinity. However, the Equation 2.12 is based on ideal components. Real components have limitations that include losses and will prevent such event to occur [21].

The average inductor current is determined by recognizing that the power supplied by the source must be the same as the power absorbed by the load, so

$$P_{IN} = P_{OUT}$$
$$V_S.I_S = \frac{V_O^2}{R_L}$$

Considering $V_S.I_S = V_S.I_L$ and V_O from Equation 2.12,

$$V_S.I_L = \frac{(\frac{V_S}{1-D})^2}{R_L} = \frac{V_S^2}{(1-D)^2 R_L}$$

solving for I_L,

$$I_L = \frac{V_S}{(1-D)^2 R_L} \tag{2.13}$$

Maximum and minimum values of the inductor current are determined by using the average value and the change in current from Equation 2.10:

$$I_{MAX} = I_L + \frac{\Delta i_L}{2} = \frac{V_S}{(1-D)^2 R_L} + \frac{V_S DT}{2L} \tag{2.14}$$

$$I_{MIN} = I_L - \frac{\Delta i_L}{2} = \frac{V_S}{(1-D)^2 R_L} - \frac{V_S DT}{2L} \tag{2.15}$$

The minimum combination of inductance and switching frequency for continuous current in the step-up converter is:

$$L_{MIN} = \frac{D(1-D)^2 R_L}{2f} \tag{2.16}$$

The preceding equations were based on the assumption that the output voltage was a constant, implying infinite capacitance. In practice, a finite capacitance will result in some fluctuation in output voltage, or ripple [21]. The expression for this ripple is

$$\Delta V_O = \frac{V_O DT}{R_L C} = \frac{V_O D}{R_L C f_s}$$

or

$$\frac{\Delta V_O}{V_O} = \frac{D}{R_L C f_s} \tag{2.17}$$

where f_s is the switching frequency.

2.8 Frequency Converter

A frequency converter is basically a device which transform an Alternating Current (AC) of one frequency to an AC with a different frequency. It uses sets of high speed switching transistors to create DC pulses that emulate the AC sine wave. These pulses not only dictate the voltage of the wave but also its frequency. In this frequency converter, the pulse-width modulation (PWM) technique to regulate the voltage and frequency is used. They are composed by four main stages: Rectifier, DC-link, Inverter and Control.

- Rectifier: composed by diodes which performs the first step of the rectification;
- DC-link: composed by a capacitor (or various), to filter the rectified current from the first stage, transforming it in a DC link;
- Inverter: composed by transistors (mostly IGBTs), converts the DC-link to an alternating current with desired amplitude and frequency;
- Control: is responsible for generating the signal that will drive the inverter and determine amplitude and frequency values of the output.

The inverter can be single or three-phase, depending on the number of arms that constitutes it. For a full-bridge single-phase frequency converter, it is necessary two arms. For three-phase applications, three arms are needed. Figure 2.11 shows a three-phase inverter.

The operation of the inverter is based on the driving of the insulated gate bipolar transistor (IGBT) by PWM. This type of signal works variating the duty-cycle of the signal. To obtain a sinusoidal waveform on the output, a sinusoidal PWM signal controls the gates of the IGBTs (Figure 2.12).

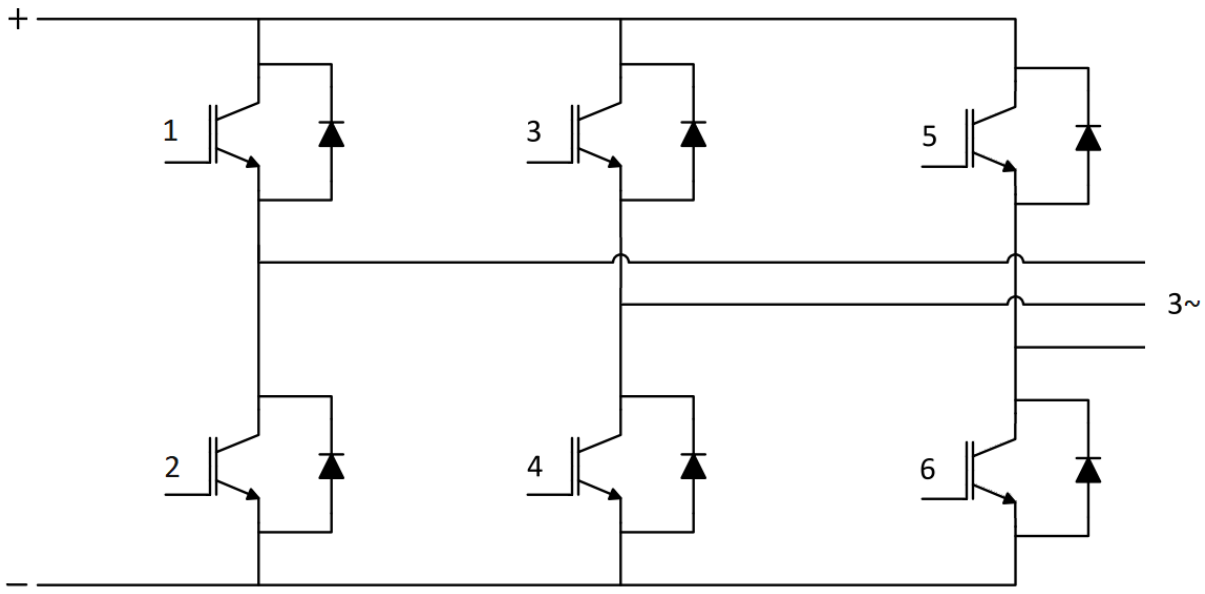

Figure 2.11: Three-phase inverter.

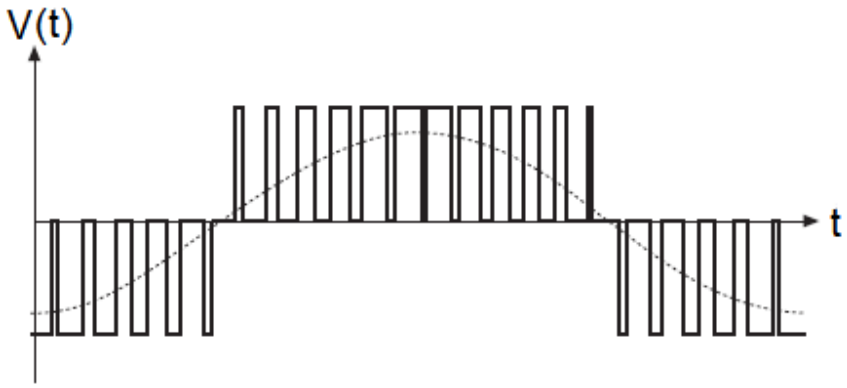

Figure 2.12: Sinusoidal PWM.

The PWM control signal has a fixed amplitude and variating duty-cycle, making possible to control the frequency and amplitude of the output.

2.9 Submersible Water Pumps

There are two principal kinds of pumps: centrifugal pumps and submersible pumps. Centrifugal pumps are used in above ground system. The mechanical energy of the motor rotates the blades of an impeller, which transfer the kinetic energy to the fluid as velocity

and pressure. The submersible pump is so called because it only works fully submerged on fluid. They are designed to operate in wells and beneath the ground systems. It is composed by a hermetically sealed motor and a pump body. The motor drives an impeller. When a pressure switch is turned on, the impeller begins to spin drawing water into the pump. The water is then pushed through the pump body and brought to the surface. The main difference of centrifugal and submersible pumps is that the first one sucks water out of the ground, and the submersible is designed to push water to the surface. The main advantage of submersible pumps is that it prevents pump cavitation, a problem associated with a high elevation difference between pump and the fluid surface. Submersible water pump examples are shown on Figure 2.13.

Figure 2.13: Submersible water pump (adapted from [22]).

2.10 Challenges of Photovoltaic Water Pumping

The use of PV energy for water pumping has been progressively implanted in several countries around the world as a solution for water supply [8]. Currently, different systems configurations and typologies have been proposed. For example, the use of a DC motor based system for the water supply problem in remotes zones of Morocco [23], a permanent magnet synchronous motor for a standalone PVWPS [24] and a three-phase induction motor PV system used for irrigation in Iraq [25].

According to the literature, these systems can be classified in two main categories: DC or AC motor driven [5]. Both categories have its own advantages and disadvantages. DC motor driven systems present high efficiency, simple control strategies and they can also be directly connected to the PV array. In contrast, they suffer from DC motor maintenance problems and limited power range. On the other hand, PVWPS powered by AC motors are more attractive for its reliability, ruggedness and low cost [26].

PV water pumping systems are composed by a PV array, an inverter and the water pump. Inverters are extensively used in industrial applications and they have been widely used in PV water pumping systems [27]. The main advantages of this approach includes technological independence and better component availability, lower cost because the components are manufactured in large quantities and increased reliability of the system because they are designed to work in industrial environments [8].

Inverters need an AC fixed input voltage and, therefore, need a minimum voltage level on its DC-link for proper operation. One initial problem is the fact that a large number of PV modules are needed to reach this minimum operating voltage. For low power systems, where the power of the motor is below 1,5 kW, this large number of PV modules implies a high value of surplus power installed. On the other hand, the number of necessary PV modules to generate the power of the pump needed implies a undervoltage value to operate the inverter. Another problem, listed in [8], is the lack of maximum power point tracking (MPPT) in standard frequency converters (SFC).

Abella et al. (2003) [27] proposed a system formed by a Standard Frequency Converter (SFC) operating in Control PID mode, with a temperature sensor on the rear face of the PV modules. The signal of the sensor generates the reference of the converters PID control.

Ramos et al. (2010) [8] proposed the implementation of a programmable logic controller (PLC) as a solution for the lack of maximum power tracking on standard frequency converters.

Miladi et al. (2014) [5] proposed an induction machine open-loop strategy of the with a converterless technique to implement the MPPT, using frequency inverters.

Parikh et al. (2017) [28] proposed a DC/DC converter to implement the MPPT on a PVWPS driven by an induction motor operating with scalar control, with validation under software simulation and tests on a resistive load.

All the works listed above showed expected results on the solutions proposed for the solar powered pumping challenges.

This chapter presented the explanation of the system , along with a solar PV energy panorama and the description of the components of the system.

Chapter 3

Control of the Power Structure

The present chapter exposes an explanation about the control methods chosen for this work. For operation of the system, the step-up converter and the single phase induction machine must be controlled, and a proportional-integrative (PI) controller and an open-loop scalar control strategy is proposed, respectively.

3.1 Proposed Solution

The system proposed is shown on Figure 3.1 and is formed by photovoltaic (PV) modules, for solar energy generation; a DC/DC boost converter (step-up) to extract the maximum power of the source (MPPT); a three arm insulated gate bipolar transistor (IGBT) inverter (one arm is used as the converters switch and diode), a single-phase submersible pump with open-loop scalar control operating mode and voltage and current sensors in all power stages of the system to perform such operation.

As showed on Chapter 2, the acquisition of the voltage (V_{pv}) and the current of the PV string (I_{pv}) are needed to perform the P&O strategy of the maximum power point tracking. The power of the PV string (P_{pv}) is obtained by multiplying V_{pv} and I_{pv}. For the open-loop scalar control of the single-phase motor, the DC-link voltage (V_{dc}) measurement is needed.

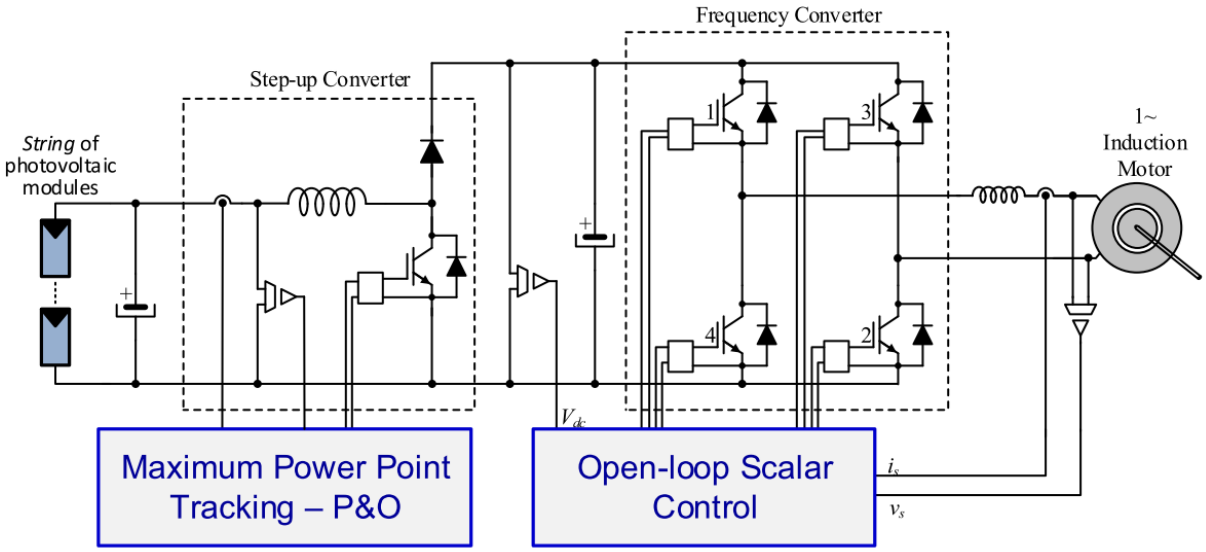

Figure 3.1: Proposed system.

3.2 Step-up Control Strategy

As explained in Chapter 2, a boost converter is basically formed by an inductor, a diode, a power switch and a capacitor. For this work, one approach is used. With a three-phase inverter, one arm of IGBTs is selected, connected to an inductor and then triggered separately, independently of the other two remaining. The higher side IGBT is left always off (open position), as it has an anti-parallel diode. It behaves basically as a diode in this case. The lower side IGBT is used as the switch of the step-up converter, with an individual control of its gate. The capacitor of the DC-link acts like the capacitor of the output of the step-up, because they have the same purpose: filtering.

Considering all this, it is possible to build a step-up converter from one arm of a three-phase inverter, by just connecting an inductor to the circuit and controlling the "switch" separately. On the other hand, the inverter looses its three-phase characteristic and will be able to drive only single phase loads. Figure 3.2 show this approach to build this type of converter from a three-phase inverter arm.

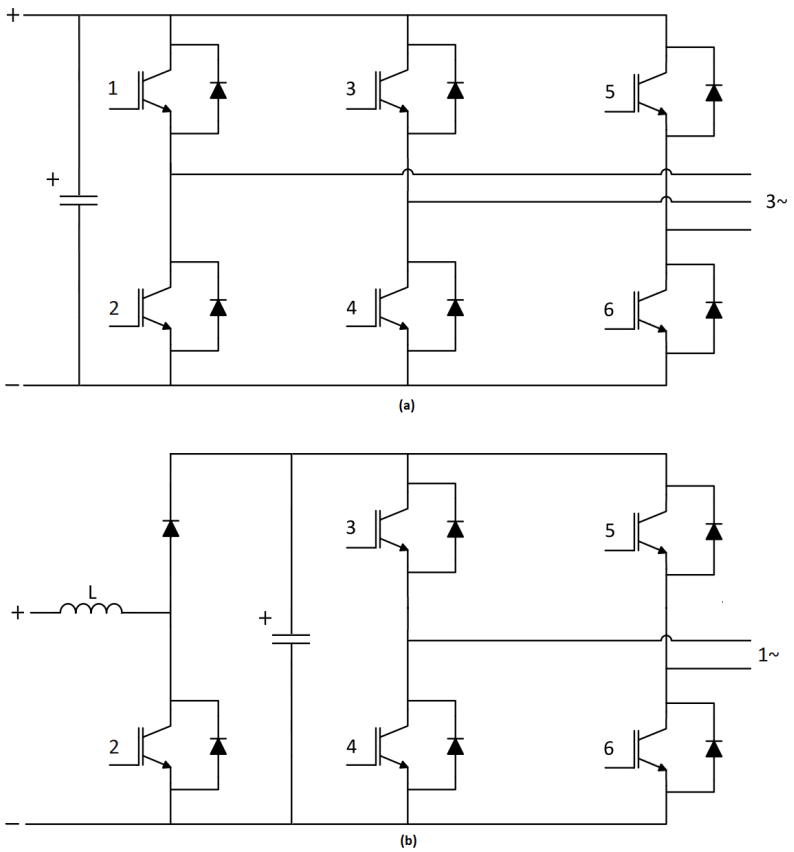

Figure 3.2: Typology of the inverter used. (a) Standard three-phase inverter. (b) Modified three-phase inverter utilized.

The step-up converter operation depends on the duty cycle value. Output voltage is defined by D as shown on equation 2.12. The maximum power operation must be ensured, and the MPPT algorithm, by reading the P_{pv} and V_{pv} values, returns on its output a positive or negative voltage increment for the reference value.

To control this system, a PI controller is projected. The controller operates as described on Chapter 2, with V_{ref} (given by MPPT algorithm) for reference. The variable of control is the duty-cycle of the step-up converter.

As the MPPT algorithm search for the maximum power operation, the PI controller imposes the system to operate on the MPP neighborhood. The K_p and K_i parameters are adjusted for system response speed and steady-state error elimination.

3.3 Induction Motor Control

The control of the induction motor is extremely important for the properly operation of the entire system. The motor behavior, as a dynamic load, must be considered in order to obtain the best functioning and the desired performance.

3.3.1 Scalar Speed Control

Scalar control, or constant V/f speed control in inverter-driven induction machines is achieved by varying the frequency fed to the motor. The voltage is varied proportionally in order to have available the rated torque on the shaft.

The speed of the induction motor is directly proportional to the frequency fed, as showing on equation 3.1.

$$n_s = \frac{120 f_{sp}}{p} \tag{3.1}$$

Where:

- n_s: rotating field or synchronous speed [rpm];
- f_{sp}: supply frequency [Hz];
- p: number of poles.

Apart from frequency, the applied voltage needs to be varied, in order to keep the air gap flux constant and not let it saturate. With this condition, the rated torque on the shaft is available [29]. The air gap induced electromotive force (EMF) in AC machines is given by

$$E_l = 4,44 K_{wl} \phi_m f_{sp} N \tag{3.2}$$

where:

- E_l: induced electromotive force [V];

- ϕ_m: peak air gap flux [Wb];
- N: number of turns per phase in the stator.

Neglecting the stator impedance, the induced EMF is approximately equal to the supply-phase voltage. Hence,

$$V_{ph} \cong E_l \tag{3.3}$$

The flux is then written as

$$\phi_m \cong \frac{V_{ph}}{K_b f_{sp}} \tag{3.4}$$

where

$$K_b = 4,44 K_{wl} T_l$$

If K_b is constant, the flux is approximately proportional to the ratio between the supply voltage and frequency. This is represented as

$$\phi_m \propto \frac{V_{ph}}{f_{sp}} \propto K_{vf} \tag{3.5}$$

Where K_{vf} is the ratio between V_{ph} and f_{sp}. From equation 3.5, to maintain the flux constant, K_{vf} has to be maintained constant. Therefore, whenever stator frequency is changed to obtain speed control, the stator input voltages, have to be changed accordingly to maintain the air gap flux constant [29].

An offset voltage V_{boost} is applied to overcome the stator resistive drop. When the machine operates with low speed, the voltage and the frequency applied are also low, to maintain the K_{vf} constant. With low voltage applied on the stator of the machine, the copper losses cannot be neglected. The relationship between the applied voltage and frequency in general is written by equation 3.6 and shown on Figure 3.3.

$$V_s = V_{boost} + K_{vf} f_{sp} \tag{3.6}$$

where $V_{boost} = I_s R_s$.

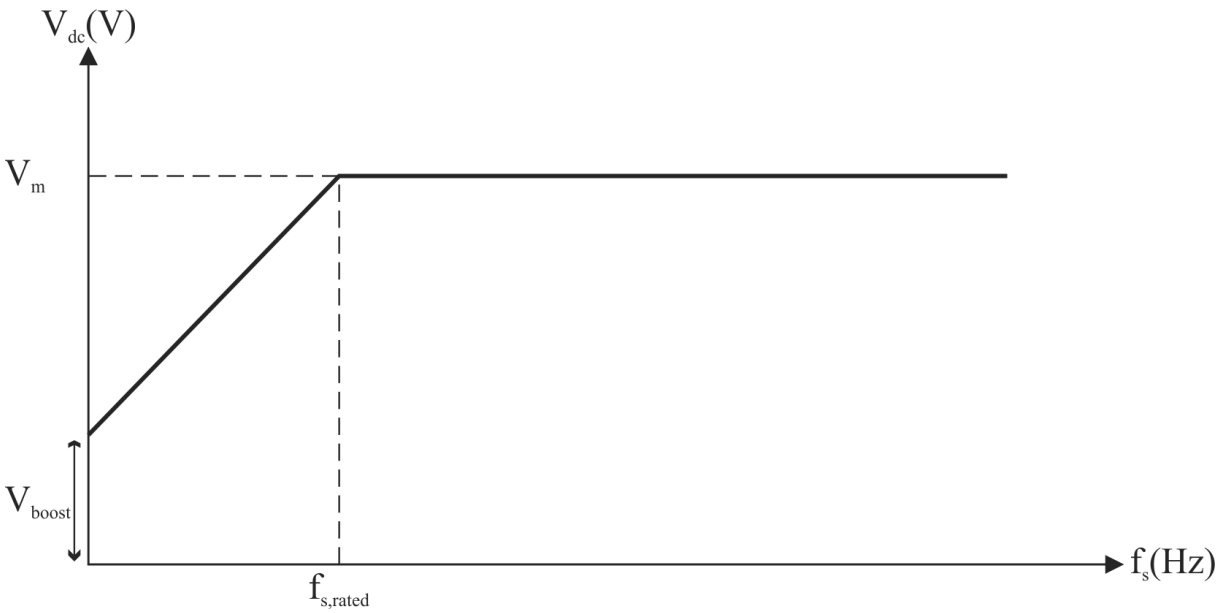

Figure 3.3: Voltage vs. frequency relationship.

3.3.2 Open-Loop Scalar Control Strategy

The proposed scalar control strategy of the induction motor is based on the DC-link voltage value. Depending on the magnitude of the V_{DC}, the maximum frequency range is decided for the required (rated) V/f ratio, as shown on Figure 3.4. During starting, the motor operates with low frequency that is ramped up at the predetermined rate. The frequency increase and decrease rates need to be adjusted according to the motor torque rating and inertia of the drive (Figure 3.4). This allows the machine to start with reduced inrush currents [30].

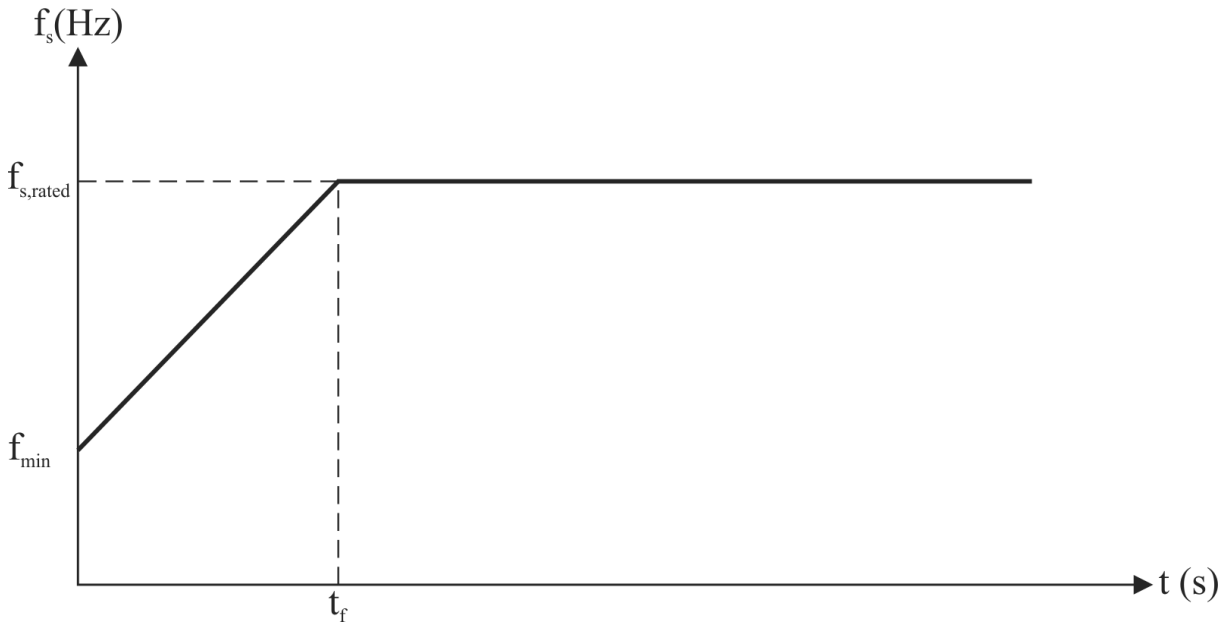

Figure 3.4: Frequency vs. time increase rate.

The open-loop scalar control scheme is shown on Figure 3.5 and implemented on Simulink (Figure 3.6). Speed command ω_e^* is obtained from the value of the DC-link. Then, from equation 3.6,

$$f_{sp} = \frac{f_{sp,rated}}{V_{m,rated} - V_{boost}}(V_s - V_{boost})$$

Since V_s maximum available is V_{dc}, then:

$$f_{sp} = \frac{f_{sp,rated}}{V_{m,rated} - V_{boost}}(V_{dc} - V_{boost}) = \frac{50}{230\sqrt{2} - V_{boost}}(V_{dc} - V_{boost})$$

or

$$\omega_e^* = \frac{2\pi \times 50}{230\sqrt{2} - V_{boost}}(V_{dc} - V_{boost})$$

as implemented on Figure 3.6.

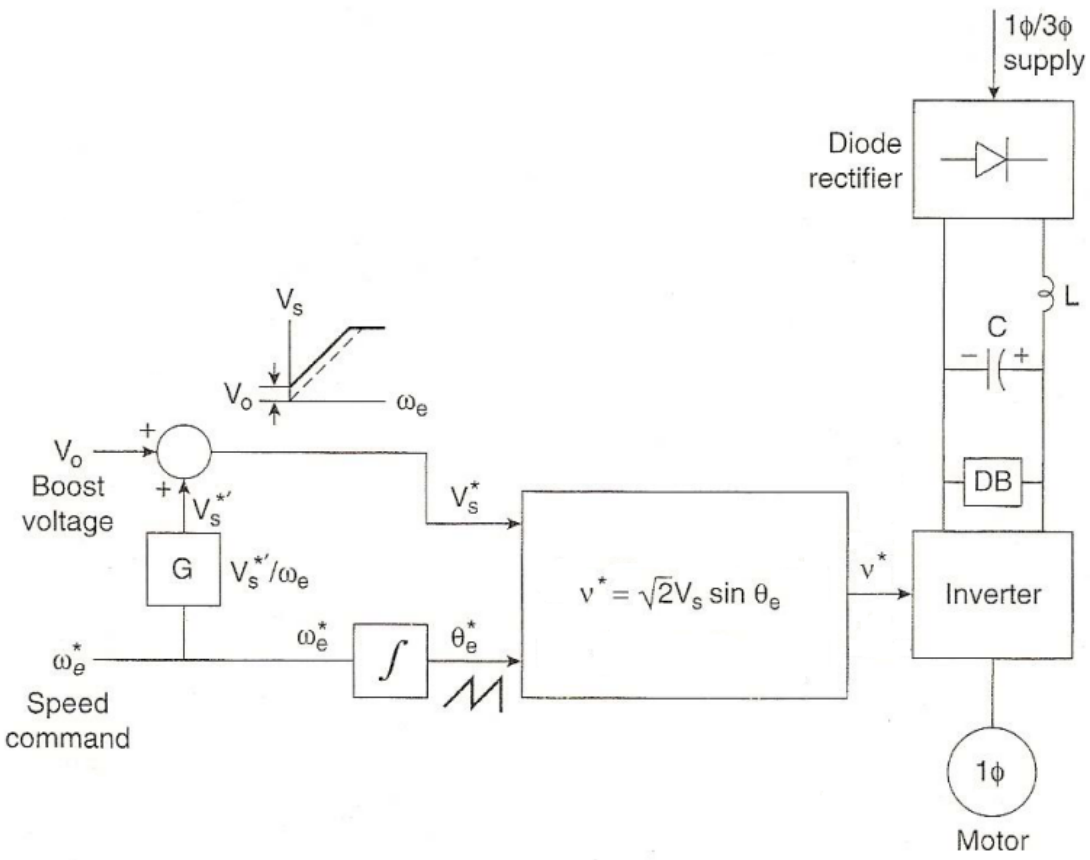

Figure 3.5: Open-loop scalar control with voltage-fed inverter [31].

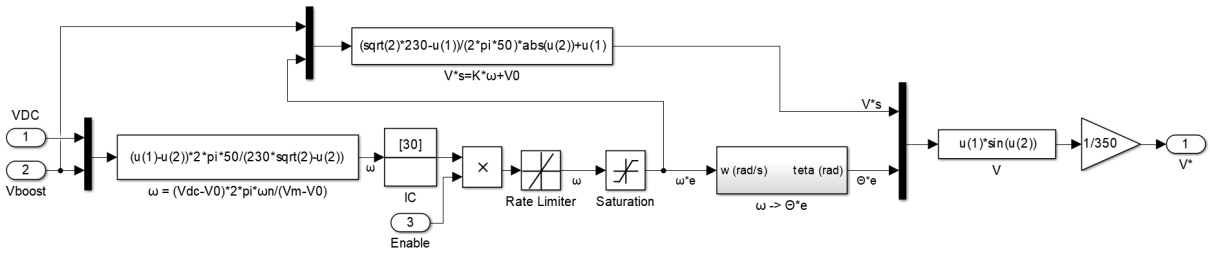

Figure 3.6: Open-loop scalar control block diagram in Simulink.

A number of control strategies have been formulated, depending on how the voltage-to-frequency ratio is implemented, such as: constant V/f control, constant slip-speed control and constant air gap flux control.

The advantages of the open-loop scalar control includes simplicity and the absence of speed encoders (because of the operation conditions of submersible water pumps) and

reduced inrush currents [32]. The disadvantage is the fact that the motor speed cannot be controlled precisely, because the rotor speed will be less than the synchronous speed, as the stator frequency is the only variable controlled in this drive and the rotor speed is not measured.

This chapter presented the strategies for the step-up converter control and the induction motor, proposing a PI controller for the step-up converter and an open-loop scalar control strategy for the motor.

Chapter 4

Simulation Results

This chapter presents results of the simulations of the step-up converter with maximum power point tracking (MMPT) implemented connected to a three-phase inverter and the results of the simulations with a single-phase induction motor fed by a photovoltaic (PV) string connected directly to a single-phase inverter.

4.1 Simulated System - Step-up Converter

The simulation of the step-up converter was achieved with the system connected to the grid. The step-up converter with MPPT algorithm system is shown on Figure 4.1. This system has six PV modules FTS-220P and the simulations were carried under three conditions of solar radiation: 700, 1000 and 600 W/m^2. In all simulations, the MPPT is performed two times per second and with a voltage increment of 2 V, under 25 °C of ambient temperature.

Figure 4.2 shows the 3 seconds window of the system the system running with G = 700 W/m^2. In Figure 4.3, the solar radiation level rises to 1000 W/m^2 at 6 seconds. As expected, the system power output as well the PV string current rises proportionally to this radiation increase. Figure 4.4 shows a drop in the radiation level to 600 W/m^2 at 8 seconds, after which the system output power as well as the PV string current decreases proportionally.

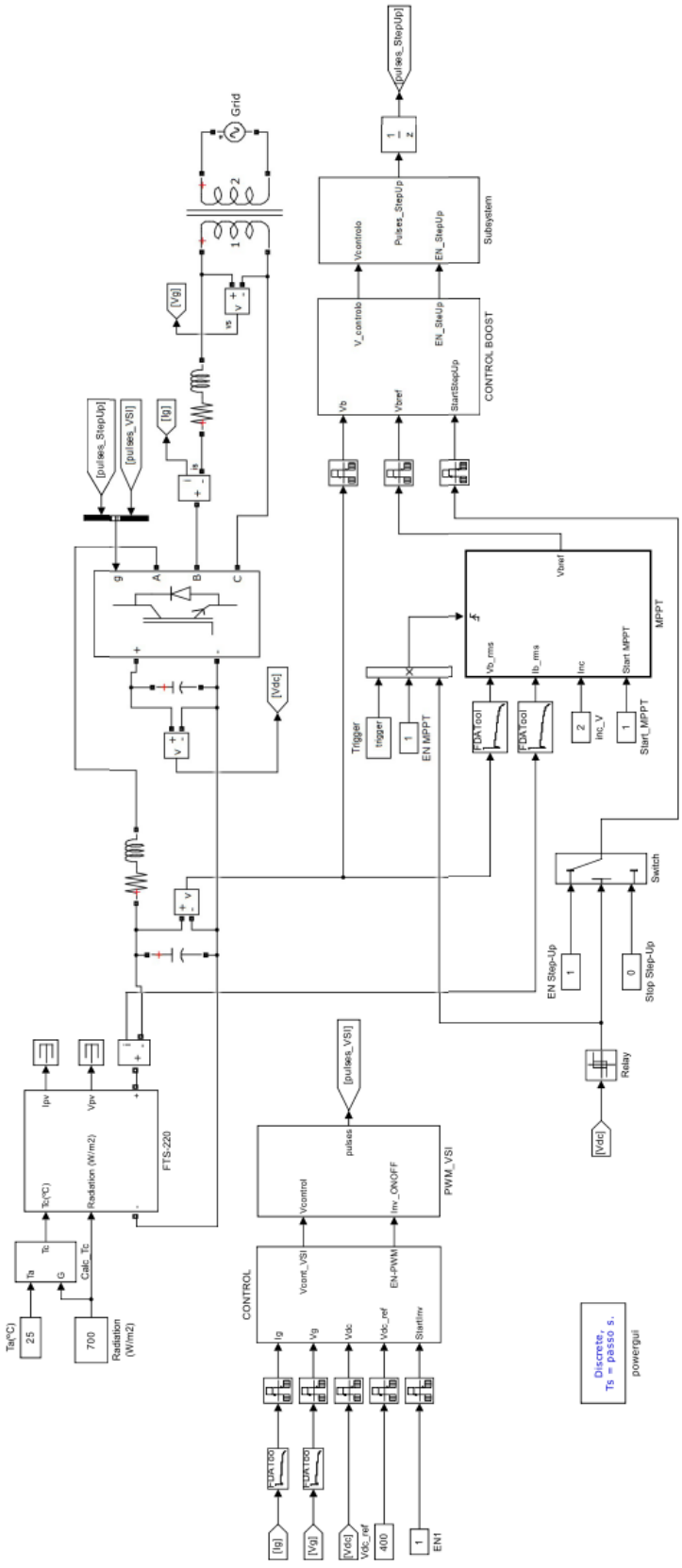

Figure 4.1: Block diagram of the step-up converter connected to the power grid.

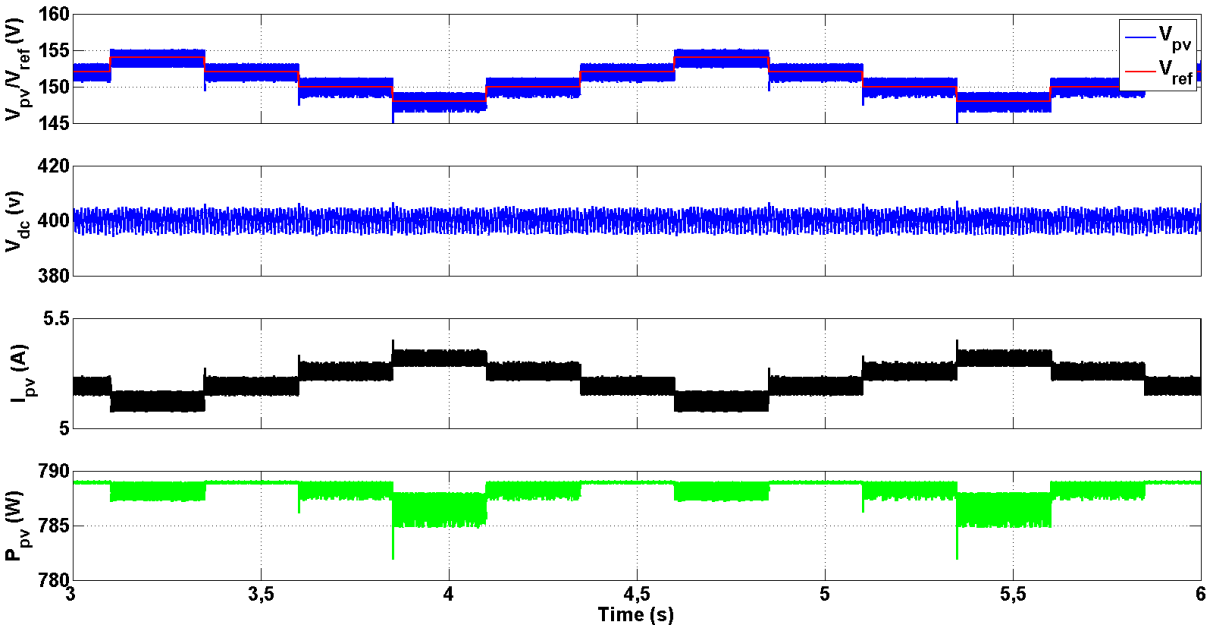

Figure 4.2: Simulation of MPPT with radiation fixed at 700 W/m^2.

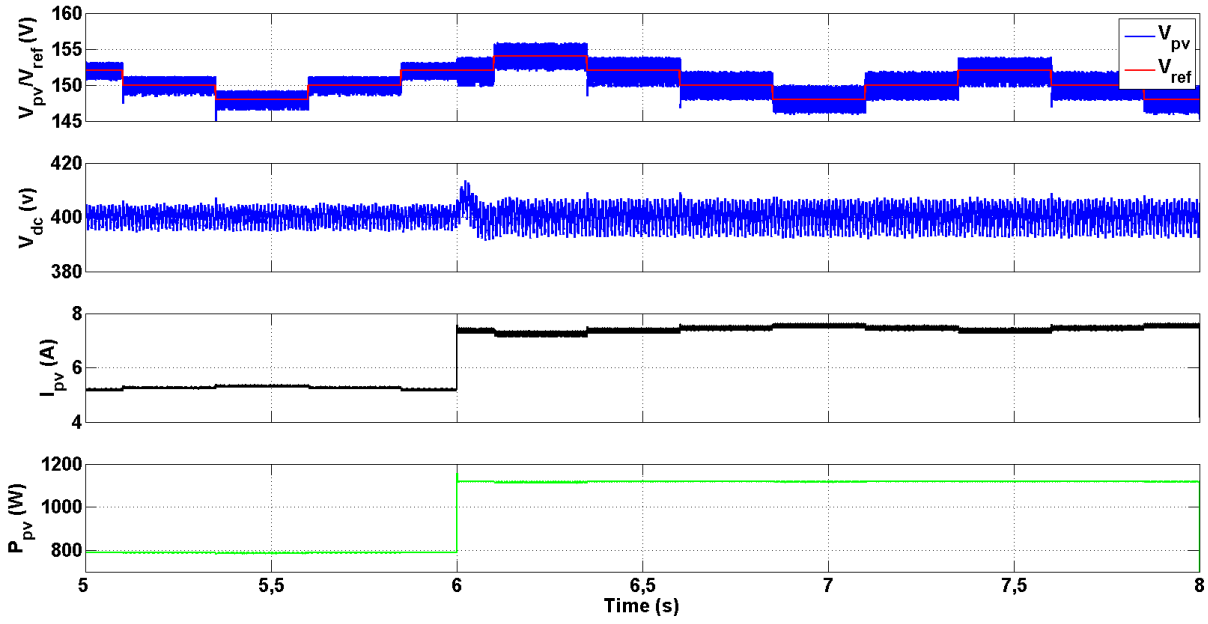

Figure 4.3: Simulation of MPPT with radiation increase from 700 to 1000 W/m^2.

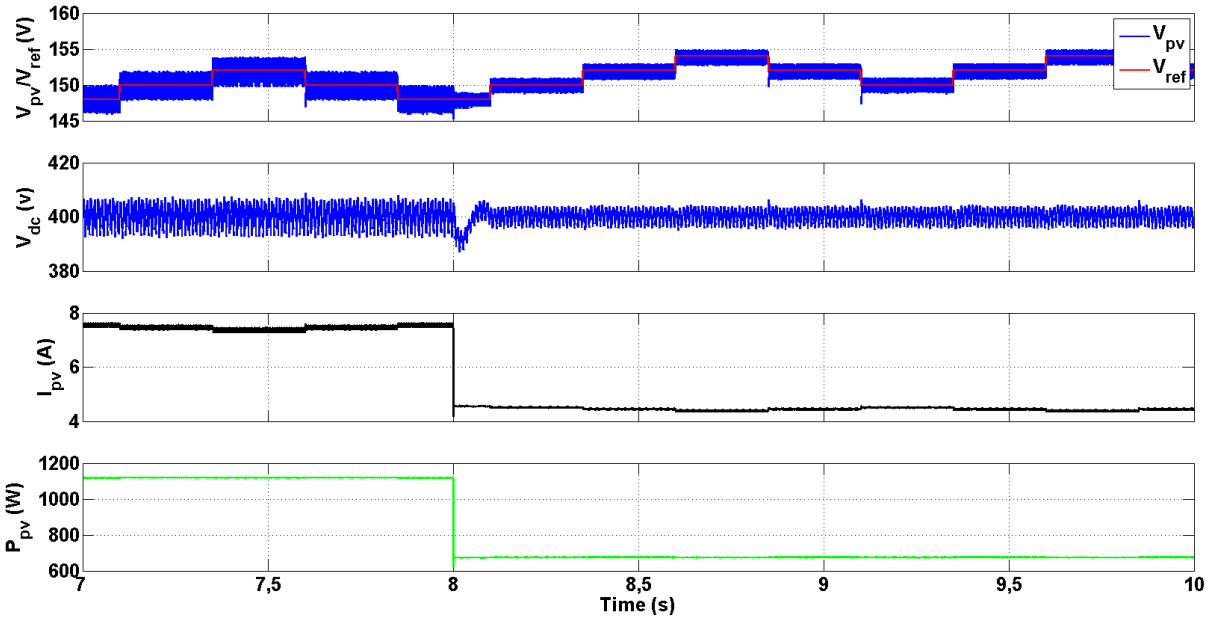

Figure 4.4: Simulation of MPPT with radiation decrease from 1000 to 600 W/m^2.

4.2 Simulated System - Single-Phase Induction Motor

The results of the proposed solution were carried under simulation on Simulink, in order to obtain the characteristic curves of voltages and currents in transient and steady-state periods under the proposed scalar control strategy.

It is important to analyze the motor inrush current, since it may reach levels of up to eight times the rated current, thus damaging the power system, control electronics and measurement circuits. The inrush current is caused by the shaft inertia and load torque during the motor starting conditions, being a critical aspect in induction machines.

Various factors affect the inrush current in this application: initial voltage on DC-link capacitor, the load torque on the shaft and the ramp of Frequency vs. Time rate, which determines how long it takes for the machine to reach its rated speed (rated frequency). The inrush current is indirectly proportional to the ramp rate.

In order to evaluate the behaviour of the induction machine with scalar control, the

system simulated showed on Figure 4.5 presents only the PV generation connected directly to the inverter.

The absence of the step-up controller is due to the incompatibility between continuous and discrete simulation algorithms used in Simulink. The static converter simulation is based on discrete domain simulation and the induction motor on a continuous domain simulation. The system is simulated here with 10 PV modules, in order to obtain the minimum voltage required for the operation of the single-phase inverter.

4.3 Simulation Parameters

The block diagram of the simulated system is shown on Figure 4.5 and the block diagram of the open-loop scalar control strategy utilized is showed by Figure 4.6. The parameters and test conditions utilized for the simulations are presented below on Table 4.1.

Table 4.1: Simulation parameters.

Parameter	**Value**
PV Modules	FTS-220P
Number of PV Modules	10
Ambient Temperature (T_a)	25°C
Radiation Level	600∼1000 W/m^2
DC-link Capacitor	2 mF
DC-link Capacitor Initial Voltage	300 V
V_{boost}	40 V
Load Torque (T_L)	5 N.m
Ramp-up Time	5 s

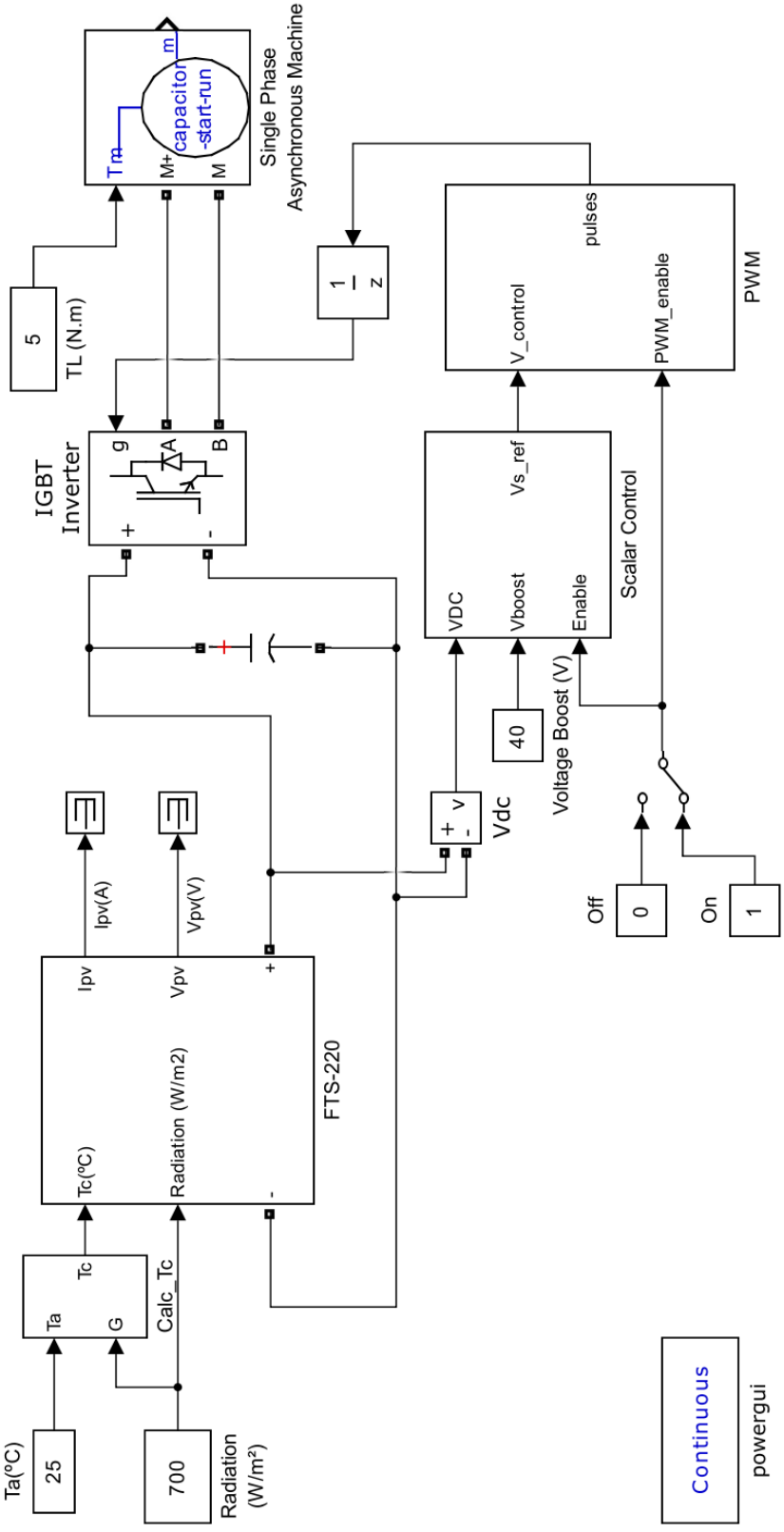

Figure 4.5: Simulated system.

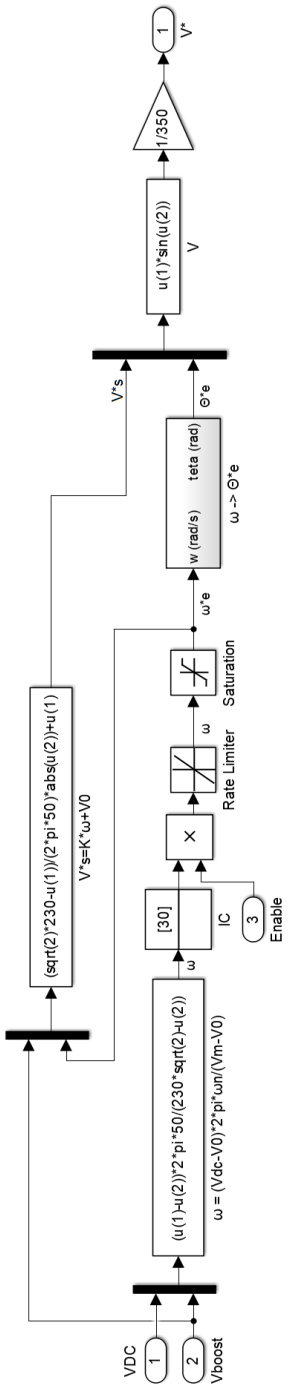

Figure 4.6: Open-loop scalar control block diagram.

The parameters of the single-phase motor are shown on Table 4.2 [33].

Table 4.2: Single-phase induction motor parameters [33].

Parameter	**Value**
Motor Type	Single-Phase Capacitor Start-Run
Voltage	220 V
Frequency	50 Hz
Power	746 W
Rated Torque	5 N.m
Pole Pairs	2
Main Winding Stator Resistance	4,02 Ω
Main Winding Stator Inductance	8,54 mH
Main Winding Rotor Resistance	2,12 Ω
Main Winding Rotor Inductance	3,12 mH
Main Winding Mutual Inductance	180 mH
Auxiliary Winding Stator Resistance	5,22 Ω
Auxiliary Winding Stator Inductance	9,54 mH
Inertia	0,0354 Kg.m^2
Friction Factor	0 Nms
Turn Ratio (aux/main)	1,18
Capacitor-Start Capacitance	150 μF
Capacitor-Start Resistance	2 Ω
Capacitor-Run Capacitance	21,5 μF
Capacitor-Run Resistance	18 Ω
Disconnection Speed (% synchronous speed)	75 %

4.4 Simulation Results

The simulation results were carried according to the system parameters listed above. All simulation results on this section shows on each figure:

- Motor Voltage (V_m [V]): the output voltage of the inverter (PWM) in blue and the motor voltage in red;
- Motor Currents (I_{main}/I_{aux} [A]): the main winding current in blue and the auxiliary winding current in red;
- Motor Speed (N [rpm]);
- Electromagnetic Torque (T_e [Nm]).

Figure 4.7 shows steady state period of the system on a window of 0,1 second of simulation, under G = 700 W/m^2, T_L = 5 Nm and T_a = 25°C.

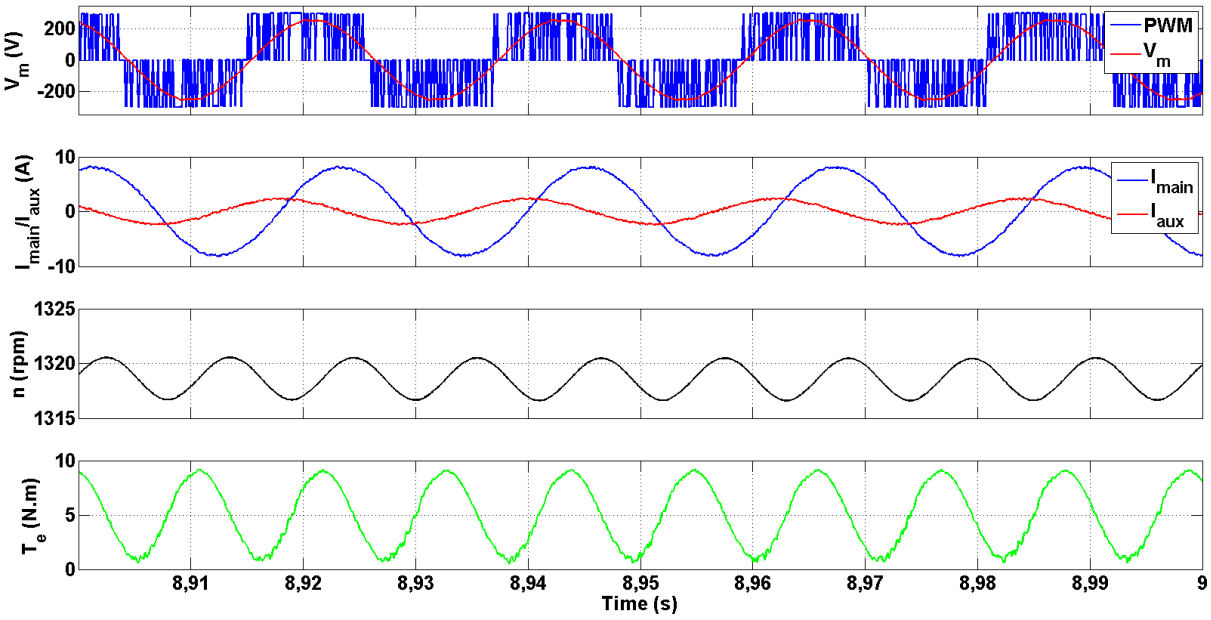

Figure 4.7: Operation of the system with G = 700 W/m^2, T_a = 25°C and T_L = 5 Nm.

The transient period of Figure 4.7 are shown in Figure 4.8. The window shown is between 0 and 3 seconds.

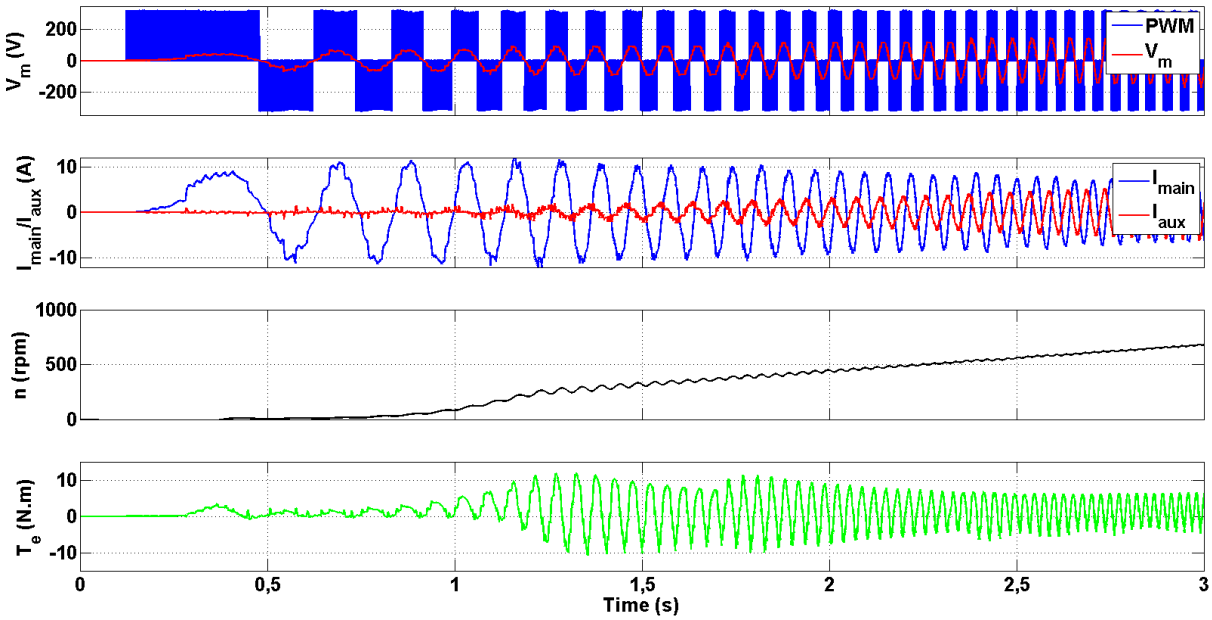

Figure 4.8: Zoom of transient period of Figure 4.7.

For comparison, Figure 4.9 shows a the difference between the transient periods of

direct start and scalar control of the motor in a 3 seconds window.

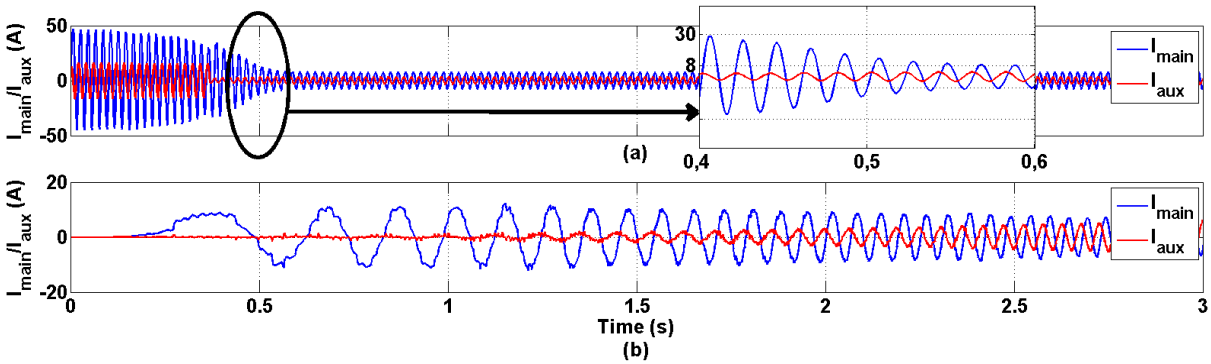

Figure 4.9: Comparison between inrush currents. (a) Direct start (with 0,4 to 0,6 second window zoom). (b) Scalar control.

As noted, the motor takes more time to start but the scalar control highly reduced the inrush current compared with the direct start.

To evaluate and validate the control of the motor, the variation of radiation and torque were simulated. Figure 4.10 shows the behaviour of the system when radiation level rises from 700 W/m^2 to 1000 W/m^2 at 8 seconds and then drops to 600 W/m^2 at 9 seconds (Figure 4.11), with $T_a = 25°C$ and $T_L = 5$ Nm.

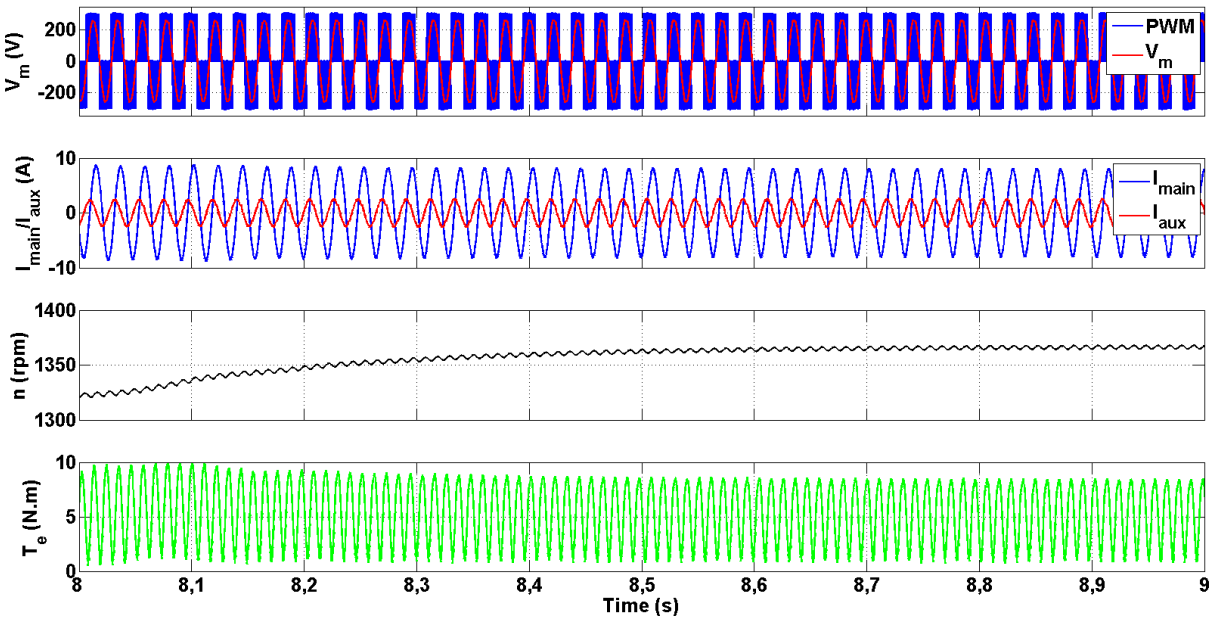

Figure 4.10: System simulation with radiation variation.

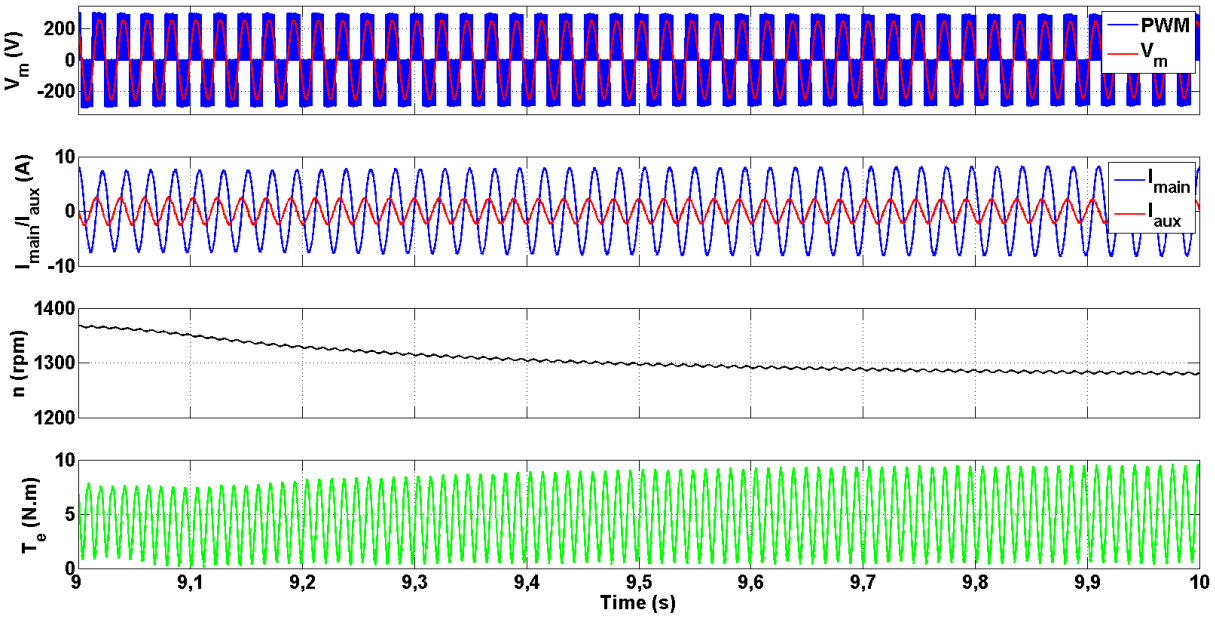

Figure 4.11: System simulation with radiation variation.

Figure 4.12 shows the system with fixed radiation level of 700 W/m^2 and a load torque variation from 5 Nm to 2,5 Nm at 7 seconds.

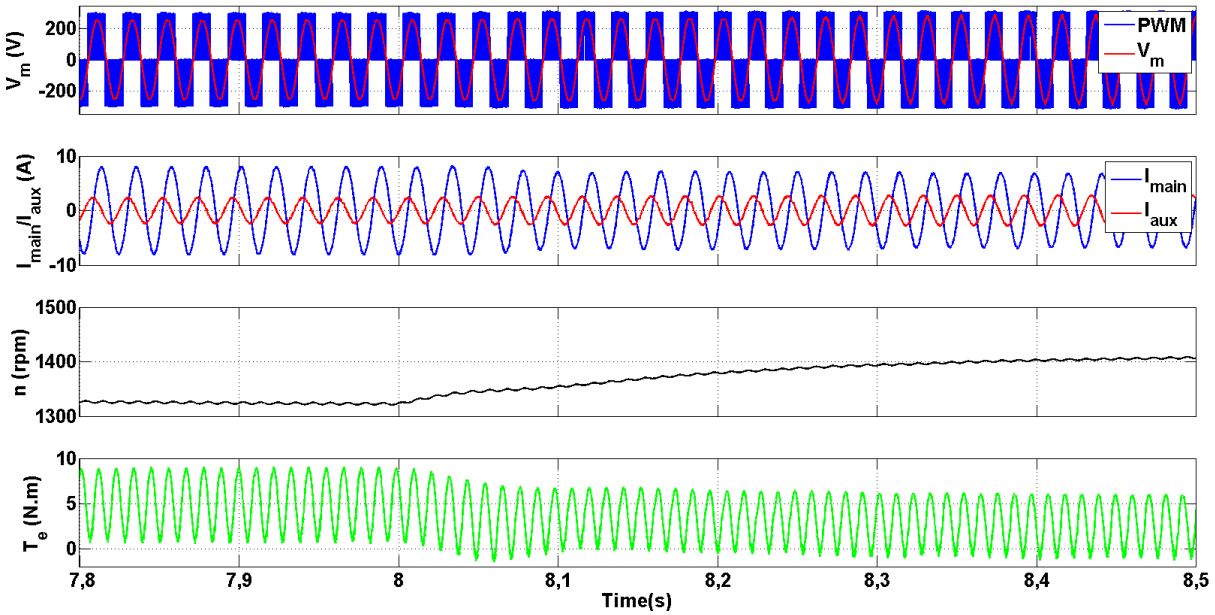

Figure 4.12: System simulation with torque variation.

The behaviour of and performance of he simulated system are the expected, under the

conditions of radiation and load torque variation. It is noticed the reduction of the inrush currents and the validation of the scalar control strategy proposed. The motor speed varies according to the voltage level on the DC-link, depending on the power available on the invert input. The step-up converter function is to extract the maximum power available at the generation and provide it on for the inverter, so the scalar control based on the voltage level on the DC-link is a way to perform the induction machine control using an open-loop strategy.

Next chapter presents the evaluation and validation of the proposed solution with simulations and experimental tests.

Chapter 5

Evaluation and Experimental Validation

The present chapter presents the experimental tests performed on software Matlab/Simulink and on a real platform to evaluate the functioning of the MPPT and validate the operation of the system's dynamics.

5.1 Experimental Validation

This work proposes the use of a DC/DC boost converter to implement the MPPT for a water pumping system. The step-up converter with maximum power point tracking (MPPT) algorithm has a dynamic response to the variation of the input parameters, in this case P_{pv} and V_{pv}.

By the fact of the inrush currents magnitude of the pump reaches up to 15 A, the experimental validation was carried out using the ABB ACS355 single-phase frequency converter.

The step-up converter is composed by an inductor, a diode and a power switch. The Powerex IPM PM75RLA120 power module was used in the building of the step-up. The PM75RLA120 is a intelligent power module that contains, on its circuit, a three-phase inverter conditioning circuits for power and operation (IGBTS, drivers and so on) [34].

With the dSPACE DS1103 PPC Control Board [35] and the real-time interface on Control Desk, the driving, controlling, measurement and protection of the converter was performed. V_{pv}, I_{pv}, V_{dc} and P_{pv} was acquired in order to perform the MPPT algorithm and the circuit protection.

A circuit protection is necessary because the step-up is switched on before the standard frequency converter (SFC) starts the driving of the motor. Therefore, in this transition, the current extracted of the converter by the SFC is null, causing a rapidly rise on the voltage on the DC-link and can cause damages to the SFC. The circuit protection for this case is simple and consists in the adding of an exception on the control block diagram. In this application, if V_{dc} rises to values higher than 480 V, the step-up is disabled until V_{dc} drops to values below 460 V. This guarantee the operation of the converter in the desired region and the protection of the SFC.

The step-up performs the MPPT algorithm with a determined frequency, and the PID macro of the SFC adjusts the speed of the pump to maintain the voltage on the DC-link equal to reference (V_{SP}). V_{SP} was fixed at 300 V (rated operation). One challenge is the adjust of the dynamics between the two power stages: the step-up converter and the SFC. Hence, the PID macro parameter's K_p and T_i, acceleration and deceleration time of the SFC, must be adjusted to match the dynamics between these two power stages. According to the tests achieved on the experimental platform, the values of these parameters used in this work are show on Table 5.1.

Table 5.1: Parameters values utilized for tests.

Parameter	**Value**
Step-up PI Controller	$K_p = 500\text{x}10^{-6}$; $K_i = 0{,}10$
SFC PID Controller	$K_p = 0{,}2$; $T_i = 2$ s; $T_d = 0$
SFC Acceleration time	0.1 s
SFC Deceleration time	0.1 s

One important aspect of these parameters is the switching frequency of the pulses for the duty-cycle of the converter. A higher switching frequency implies a lower value of

the inductor, as explained in the DC/DC converters section in chapter 2. In this work, a switching frequency of 10 kHz was utilized, but higher frequency values are interesting for research in order to decrease the size of the inductor for the step-up.

5.2 Experimental System

To analyze the operation of the MPPT system and the load, simulations of the step-up with MPPT on Simulink platform of Matlab and then tests performed on a real experimental platform with PV modules, standard frequency converter and a submersible water pump.

To evaluate and validate the functioning of the system, tests on a real platform composed by PV modules, SFC and a submersible water pump were performed. The system electric scheme is shown on Figure 5.1.

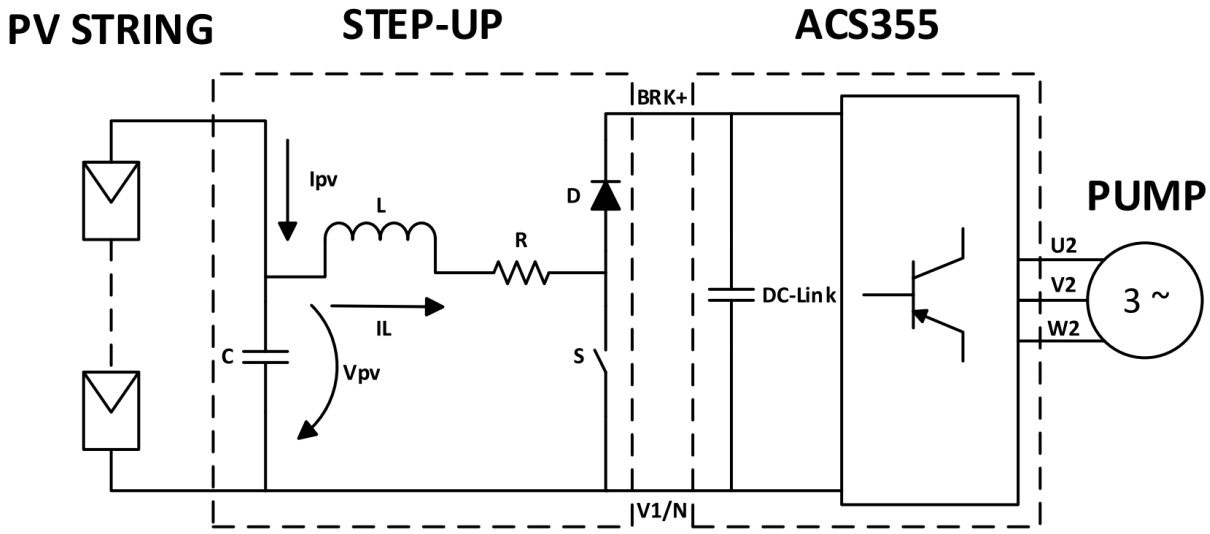

Figure 5.1: Electric scheme of the system utilized.

The system is shown on Figure 5.3 and is composed by the elements described on Table 5.2. A three-phase pump is used because of the non-availability of a frequency converter with a single-phase output.

The PV modules (Figure 5.3-a) are installed on the roof of the laboratory. In total,

9 PV modules are available, and a connection box present in the laboratory allows the build of a string with the desired number of PV modules. The step-up is shown on Figure 5.3-b. The set-up of the step-up using the dSPACE DS1103 PPC control board is shown on Figure 5.2. The SFC ABB ACS355 and the pump with the water tank are shown on Figures 5.3-c and 5.3-d, respectively. Figure 5.5 shows the Control Desk interface utilized.

Table 5.2: Components of the system.

Component	**Equipment Used**
Pump	Termar B20 3∼ 1.5 kW - 2 HP Submersible
Standard Frequency Converter	ABB ACS355-01E-07A5-2
Step-up Power Switch and Diode	Two IGBTs of Mitsubishi PM75RLA120
Step-up Inductor	Mundorf BT140 12 mH/0,45 Ohm
Photovoltaic Modules	Fluitecnik's FTS-220P

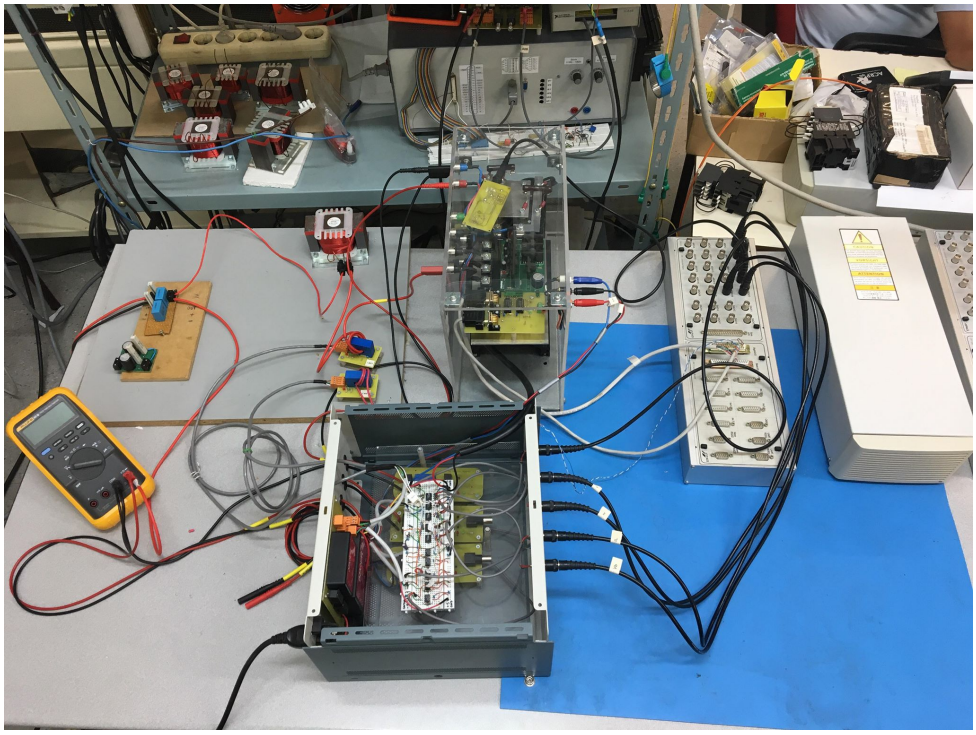

Figure 5.2: Complete set-up of the step-up converter (components and control).

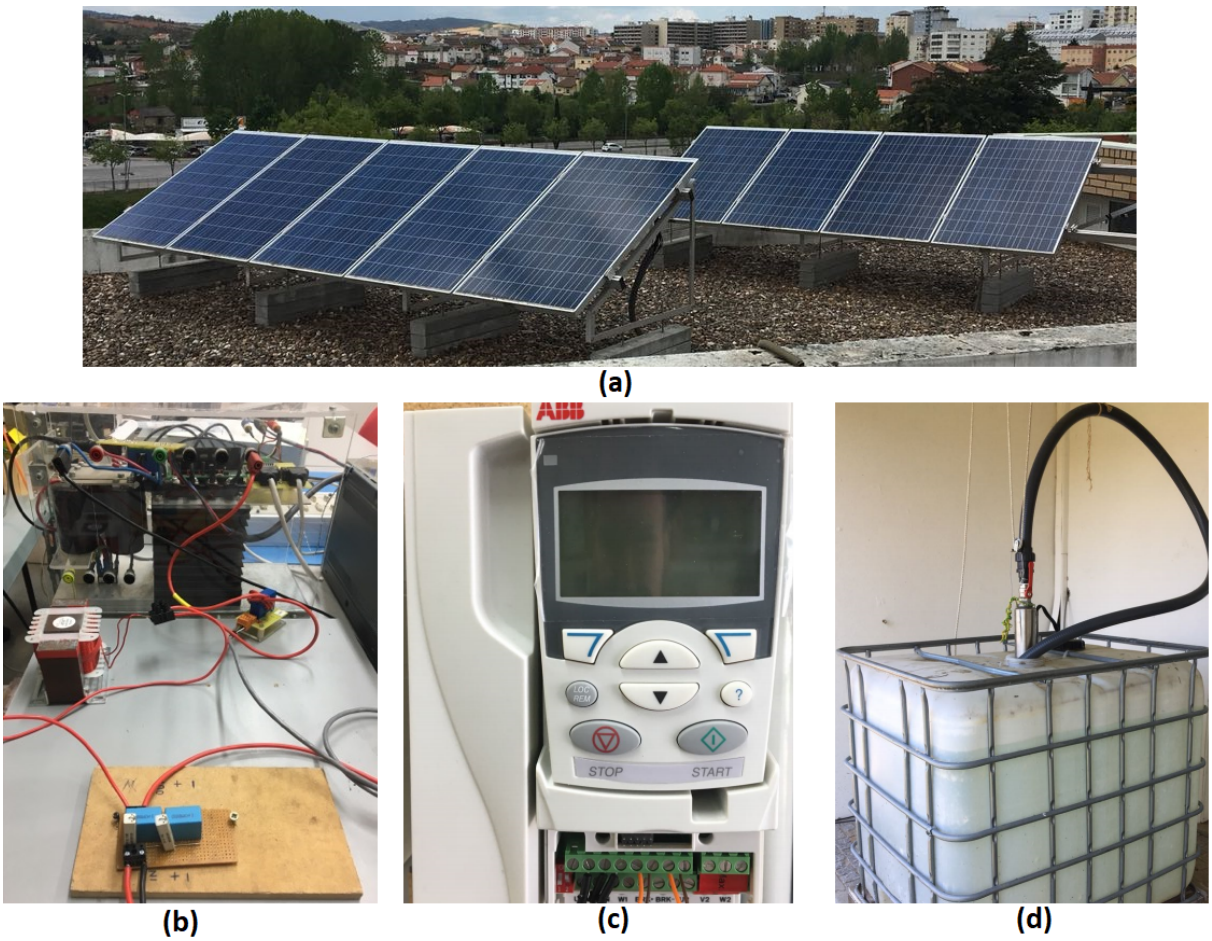

Figure 5.3: Experimental platform, (a) PV string, (b) step-up converter, (c) single-phase standard frequency converter, (d) water tank and pump.

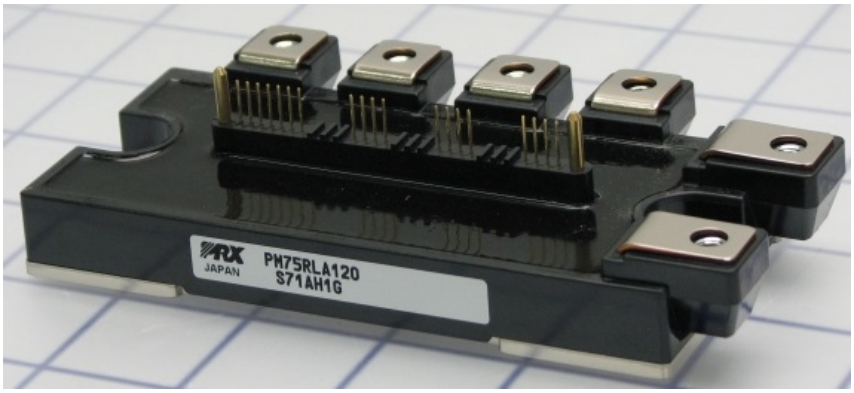

Figure 5.4: Powerex intelligent power module PM75RLA120 [34].

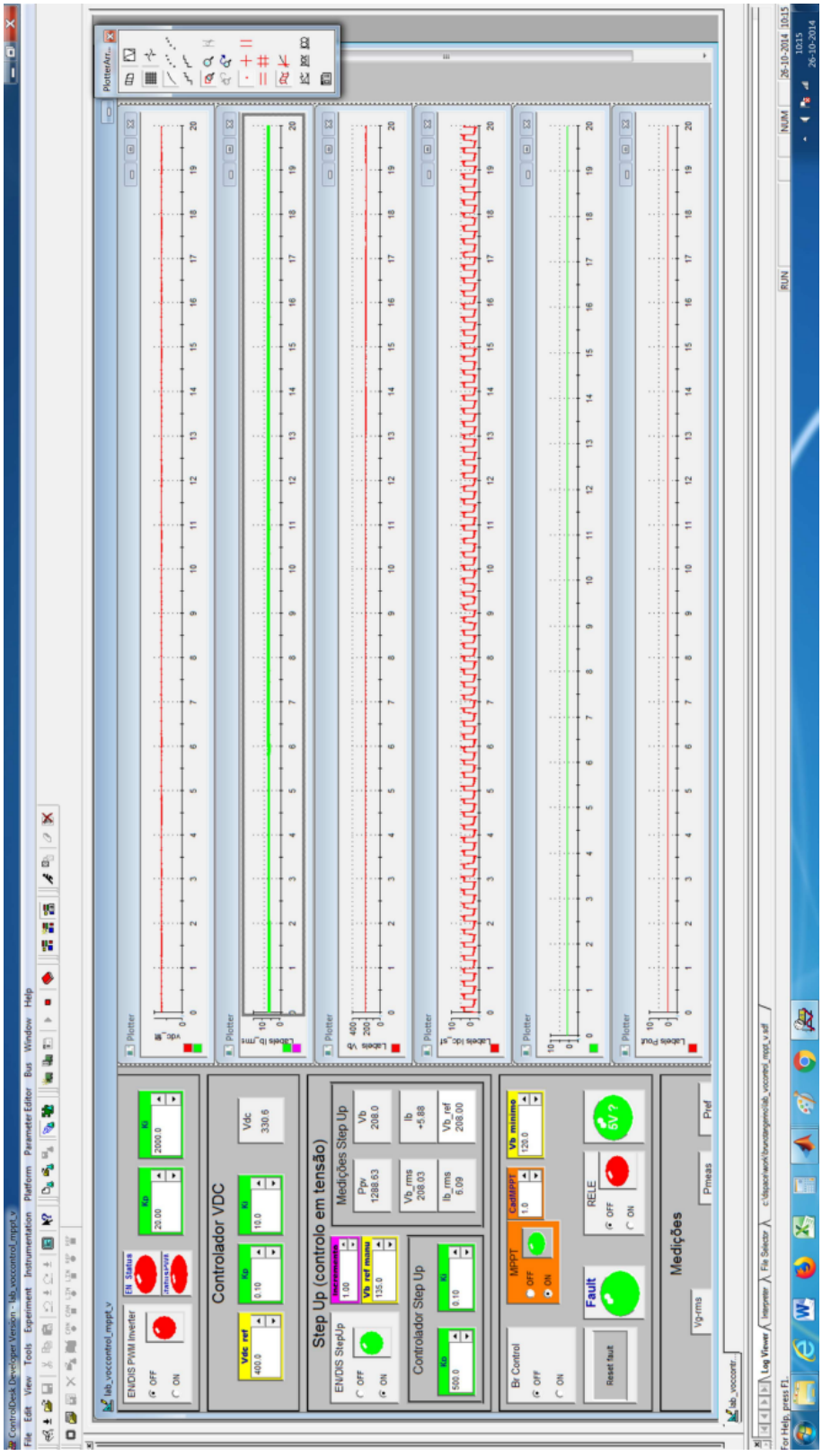

Figure 5.5: Control Desk interface.

5.3 Experimental Results

The experimental results were carried out with 4, 6 and 8 PV modules available on the roof of the laboratory. All tests were performed under same solar radiation and temperature levels, acquired by the measuring system present in the laboratory (Table 5.3).

Table 5.3: Comparison of the power and voltage of each set.

Condition	**Value**
Date and Time	07/05/2018 - 11:00
Radiation level	G = 810 W/m^2
Ambient Temperature	T_a = 28°C
PV Module Temperature	T_{pv} = 45°C

The results Figures 5.6, 5.7 and 5.8 show the V_{pv}, V_{dc}, I_{pv} and P_{pv} curves for 4, 6 and 8 PV modules, respectively. V_{SP} was set 300 V and the MPPT is running two times per second with voltage increment of 1 V.

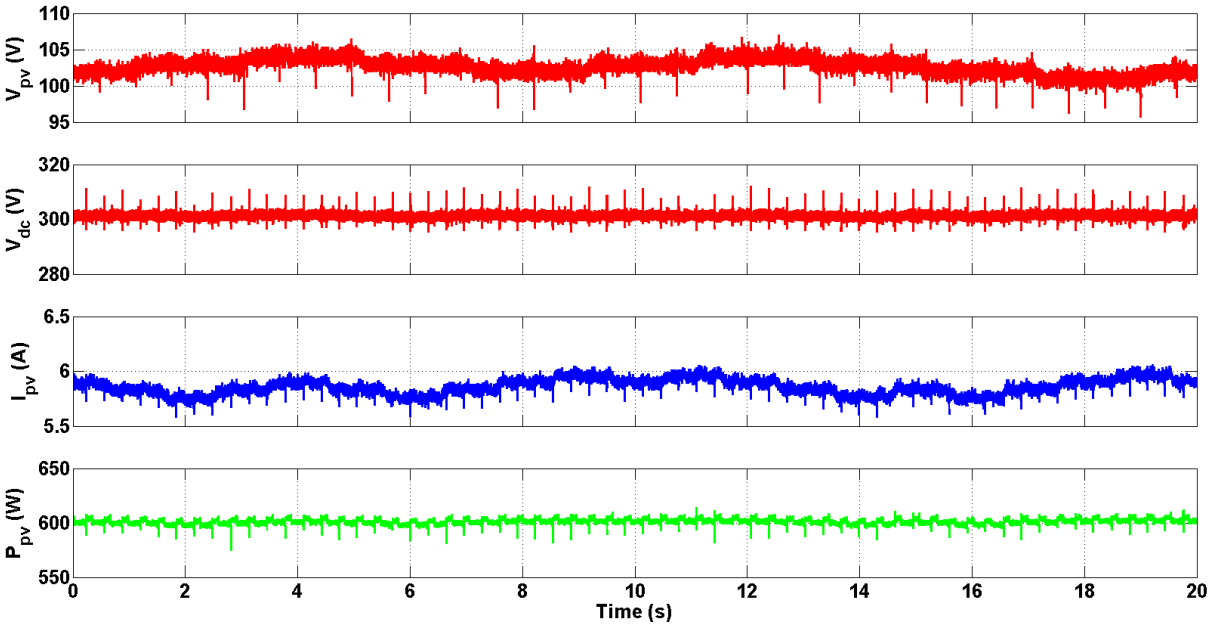

Figure 5.6: V_{pv}, V_{dc}, I_{pv} and P_{pv} for 4 PV modules.

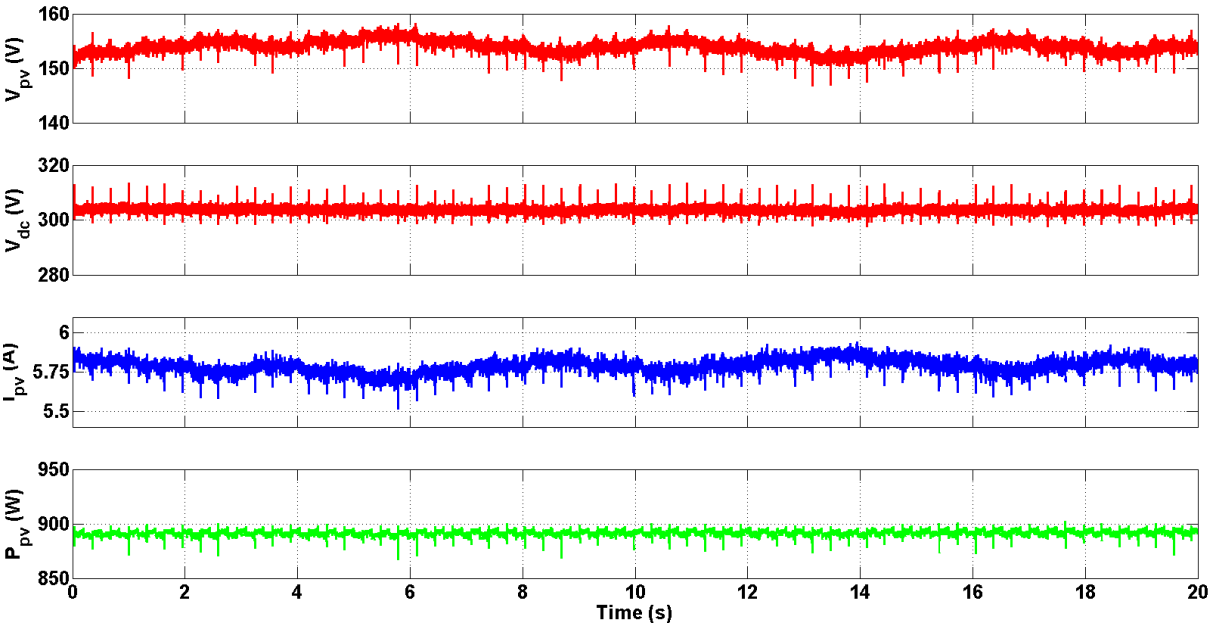

Figure 5.7: V_{pv}, V_{dc}, I_{pv} and P_{pv} for 6 PV modules.

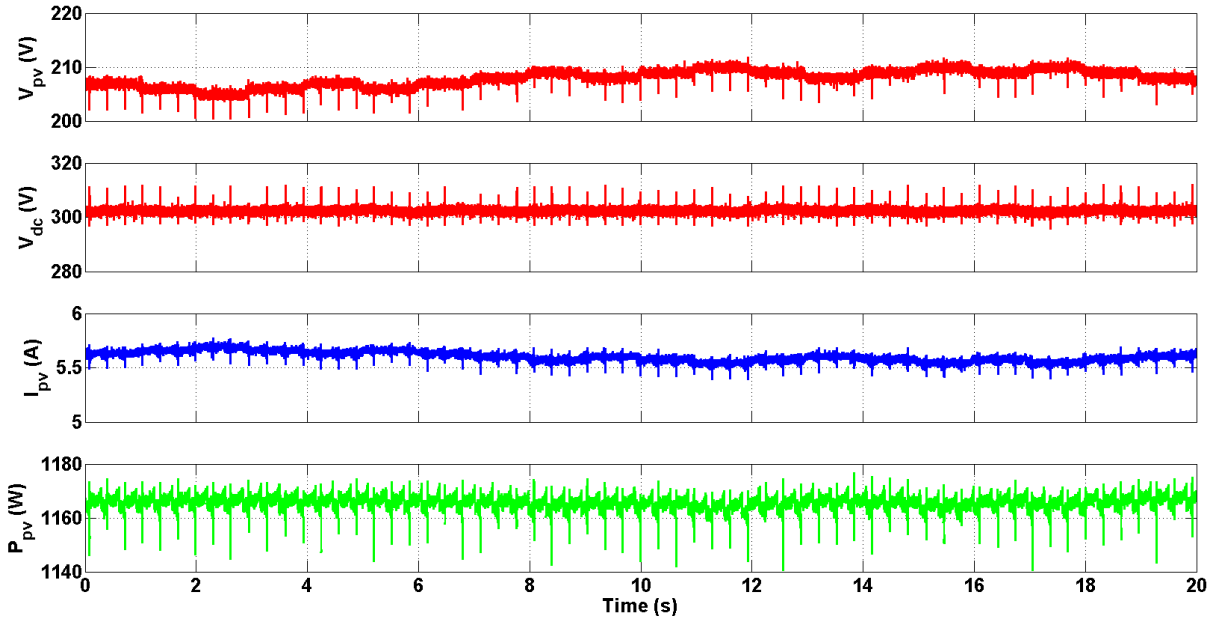

Figure 5.8: V_{pv}, V_{dc}, I_{pv} and P_{pv} for 8 PV modules.

For all conditions V_{dc} is 300 V and V_{pv} varies according to the MPPT algorithm and the behaviour on the simulated system and the real platform system parameters are equivalent, validating this way the parameters of PID controller of the SFC and the match

between these two systems dynamics. The power curve as the water pump operating show expected results for the operation of the system. To solve the problem of the number of PV modules on low power systems and the implementation of a MPPT, the addition of DC/DC converter has been proven to operate as expected. The validity of these proposals has been evaluated experimentally in a real system.

This chapter showed the evaluation and validation of the proposed solution of the step-up converter with MPPT implemented in real conditions tests with a SFC and submersible pump.

Chapter 6

Conclusions and Future Works

This work presented solutions for the mentioned challenges in photovoltaic water pumping system (PVWPS). On this chapter the conclusions and future works for the control strategies proposed on the scope of PVWPS are presented.

6.1 Conclusions

A control method for the step-up converter as a solution for two relevant PVWPS challenges and a control method for single-phase induction motors using an open-loop scalar control.

The implementation of a step-up converter showed a satisfactory solution for the oversizing on the number of installed photovoltaic (PV) modules to power PVWPS and the lack of maximum power point tracking in standard frequency converters. The simulations and experimental results showed the expected performance of the system under tests conditions. One challenge of this solution was to adjust the parameters of the standard frequency converter (SFC) in order to match the dynamics between the step-up converter and the SFC, as the motor dynamics (mechanical quantities) is slower compared to the voltage and current variation of the converter (electrical quantities).

This work also proposed an open-loop scalar control strategy for single-phase induction motors, which indirectly controls the speed and the voltage of the machine in order to

start the motor with reduced speed and ramp-up to rated value to avoid high values of inrush current and keep the V/f ratio constant to maintain the rated torque on the shaft available. The simulations under the conditions tested showed satisfactory results. The challenges of this strategy was the fact that only the voltage and the current of the motor was available to perform the control, making it simple for implementation but on the other hand the speed is indirectly controlled by variating the frequency fed to the motor.

The control methods showed satisfactory results and reached the objectives of the work to solve the oversizing challenge PVWPS, the lack of maximum power point tracking in standard frequency converters on the step-up scope and the inrush current and the speed control performing using only voltage and current of the motor. PVWPS based on conventional components presents high reliability, ruggedness and lower maintenance rate compared to PVWPS based on DC motors. The results of the experimental validation were used to write an article which was submitted to the Ibero-American Congress of Smart Cities (ICSC-CITIES 2018). The article is shown on appendix A.

6.2 Further Developments

Throughout this work, two control methods were proposed. The implementation of the step-up converter showed satisfactory results, and for futures works, the optimization in the inductor by changing the switching frequency implies in a lower values of inductance required, lowering the volume of the circuit and consequently the cost of the component.

The open-loop scalar control was simulated using a 746 W capacitor start-run induction motor, and for future works developments, the optimization of the frequency ramp-up for inrush current and starting time reduction, and the application of this strategy on other types of single-phase induction motors, as split-phase and permanent split capacitor (PSC) are interesting.

Bibliography

[1] J. V. M. Caracas, G. d. C. Farias, L. F. M. Teixeira, and L. A. d. S. Ribeiro, "Implementation of a high-efficiency, high-lifetime, and low-cost converter for an autonomous photovoltaic water pumping system", *IEEE Transactions on Industry Applications*, vol. 50, no. 1, pp. 631–641, Jan. 2014.

[2] M. Chunting, M. B. R. Correa, and J. O. P. Pinto, "The ieee 2011 international future energy challenge - request for proposals", *Proc. IFEC*, 2010.

[3] S. G. Malla, C. N. Bhende, and S. Mishra, "Photovoltaic based water pumping system", in *2011 International Conference on Energy, Automation and Signal*, Dec. 2011, pp. 1–4.

[4] C. Gopal, M. Mohanraj, P. Chandramohan, and P. Chandrasekar, "Renewable energy source water pumping systems—a literature review", *Renewable and Sustainable Energy Reviews*, vol. 25, pp. 351–370, 2013. [Online]. Available: http://www.sciencedirect.com/science/article/pii/S1364032113002633.

[5] M. Miladi, A. B. Abdelghani-Bennani, I. Slama-Belkhodja, and H. M'Saad, "Improved low cost induction motor control for stand alone solar pumping", in *2014 International Conference on Electrical Sciences and Technologies in Maghreb (CISTEM)*, Nov. 2014, pp. 1–8.

[6] A. U. Brito, M. C. Fedrizzi, and R. Zilles, "Pv pumping systems: A useful tool to check operational performance", *Progress in Photovoltaics: Research and Applications*, vol. 15, no. 1, pp. 41–49, 2006.

[7] M. Yaichi and M.-K. Fellah, "Centrifugal motor-pump system model intended for the photovoltaic pumping applications", vol. 89, pp. 111–115, Aug. 2013.

[8] J. Fernández-Ramos, L. Narvarte-Fernández, and F. Poza-Saura, "Improvement of photovoltaic pumping systems based on standard frequency converters by means of programmable logic controllers", *Solar Energy*, vol. 84, no. 1, pp. 101–109, 2010.

[9] S. P. Europe, *Global market outlook for solar power/2017-2021*, Solar Power Europe, Brussels, Belgium, 2017.

[10] ——, *Global market outlook for solar power/2016-2020*, Solar Power Europe, 2016.

[11] V. C. Sontake and V. R. Kalamkar, "Solar photovoltaic water pumping system - a comprehensive review", *Renewable and Sustainable Energy Reviews*, vol. 59, pp. 1038–1067, 2016.

[12] C. S. Solanki, *Solar photovoltaics: Fundamentals, technologies and applications*. PHI Learning Pvt. Ltd., 2015.

[13] D. Rusirawan and I. Farkas, "Identification of model parameters of the photovoltaic solar cells", *Energy Procedia*, vol. 57, pp. 39–46, 2014, 2013 ISES Solar World Congress, ISSN: 1876-6102.

[14] A. V. T. Leite, *Lecture notes in photovoltaic systems*, Mar. 2018.

[15] F. S. Energy, *Fluitecnik solar modules installation manual*, http://www.fluitecnik.com/default/documentos/498_en-installation_and_safety_manual.pdf, Online; acessed 20-April-2018, May 2012.

[16] S. R. Wenham, M. A. Green, M. E. Watt, R. Corkish, and A. Sproul, *Applied photovoltaics*. Routledge, 2013.

[17] N. Karami, N. Moubayed, and R. Outbib, "General review and classification of different mppt techniques", *Renewable and Sustainable Energy Reviews*, vol. 68, pp. 1–18, 2017.

[18] A. C. Zamora, G. Vazquez, J. M. Sosa, P. R. Martinez-Rodriguez, and M. A. Juarez, "Efficiency based comparative analysis of selected classical mppt methods", in *2017 IEEE International Autumn Meeting on Power, Electronics and Computing (ROPEC)*, Nov. 2017, pp. 1–6.

[19] J.-A. Jiang, Y.-L. Su, K.-C. Kuo, C.-H. Wang, M.-S. Liao, J.-C. Wang, C.-K. Huang, C.-Y. Chou, C.-H. Lee, and J.-C. Shieh, "On a hybrid mppt control scheme to improve energy harvesting performance of traditional two-stage inverters used in photovoltaic systems", *Renewable and Sustainable Energy Reviews*, vol. 69, pp. 1113–1128, 2017.

[20] D. Sera, R. Teodorescu, J. Hantschel, and M. Knoll, "Optimized maximum power point tracker for fast changing environmental conditions", in *2008 IEEE International Symposium on Industrial Electronics*, Jun. 2008, pp. 2401–2407.

[21] D. W. Hart, *Introduction to power electronics*. Prentice hall, 1997.

[22] Nochi, *Electric pumps catalog*, http://www.tumapumpen.at/upload/medialibrary/16_Katalog.pdf, Online; acessed 09-May-2018.

[23] S. Abdourraziq, M. A. Abdourraziq, and C. Darab, "Photovoltaic water pumping system application in morocco", in *2017 International Conference on Electromechanical and Power Systems (SIELMEN)*, Oct. 2017, pp. 271–274.

[24] M. Kashif, S. Murshid, and B. Singh, "Standalone solar pv array fed smc based pmsm driven water pumping system", in *2018 IEEMA Engineer Infinite Conference (eTechNxT)*, Mar. 2018, pp. 1–6.

[25] A. T. Mohsin and I. M. Abdulbaqi, "Analysis of an irrigation pump driver fed by solar pv panel", in *2018 1st International Scientific Conference of Engineering Sciences - 3rd Scientific Conference of Engineering Science (ISCES)*, Jan. 2018, pp. 92–97.

[26] S. R. Bhat, A. Pittet, and B. S. Sonde, "Performance optimization of induction motor-pump system using photovoltaic energy source", *IEEE Transactions on Industry Applications*, vol. IA-23, no. 6, pp. 995–1000, Nov. 1987.

[27] M. A. Abella, E. Lorenzo, and F. Chenlo, "Pv water pumping systems based on standard frequency converters", *Progress in Photovoltaics: Research and Applications*, vol. 11, no. 3, pp. 179–191,

[28] A. P. Parikh, P. N. Tekwani, and V. Patel, "Design and implementation of solar pumping system with induction motor and submersible pump", in *2017 Nirma University International Conference on Engineering (NUiCONE)*, Nov. 2017, pp. 1–6.

[29] R. Krishnan, *Electric motor drives: Modeling, analysis, and control*. Prentice Hall, 2001.

[30] M. Naveenkumar, A. Munjal, S. Srinivasan, and D. Prasad, "Design and implementation of a variable frequency drive for single-phase induction motor", in *2015 IEEE International WIE Conference on Electrical and Computer Engineering (WIECONECE)*, Dec. 2015, pp. 239–242.

[31] B. K. Bose and B. K. Bose, *Power electronics and variable frequency drives: Technology and applications*. Wiley Online Library, 1997, vol. 2.

[32] G. Kohlrusz and D. Fodor, "Comparison of scalar and vector control strategies of induction motors", *Hungarian Journal of Industry and Chemistry*, vol. 39, no. 2, pp. 265–270, 2011.

[33] S. H. Khader, "Modeling and simulation of single phase double capacitors induction motor", vol. 3, Sep. 2009.

[34] M. Electric, *Powerex ipm datasheet*, https://www.mitsubishielectric-mesh.com/products/pdf/pm75rla120_e.pdf, Online; acessed 23-Jun-2018.

[35] dSPACE, *Ds1103 ppc controller board*, http://www.ceanet.com.au/Portals/0/documents/products/dSPACE/dspace_2008_ds1103_en_pi777.pdf, Online; acessed 23-Jun-2018.

Appendix A

Appendix - Article

Photovoltaic Water Pumping System for Low Power Conventional AC Pumps

Bruno Tangerino[1,2], Dionízio Roman[1,2], Vicente Leite[1], Alessandro Goedtel[2], Ângela Ferreira[1], José Batista[1], and Wellington Maidana[1,2]

[1] Instituto Politécnico de Bragança, Bragança, Portugal
[2] Universidade Tecnológica Federal do Paraná, Campus Cornlélio Procópio, Paraná, Brasil
tangerino.bruno2@hotmail.com; dionizioroman@hotmail.com; avtl@ipb.pt; agoedtel@utfpr.edu.br; apf@ipb.pt; jbatista@ipb.pt; maidana@ipb.pt

Abstract. The interest of photovoltaic (PV) water pumping systems with standard components is increasing as a low cost and independent solution against dedicated systems. However, one of the challenges of this alternative is the fact that low power systems requires a small number of PV modules to drive low power pumps but the PV string voltage is not enough to feed the frequency converter. This paper shows an approach to this case with a DC/DC converter with maximum power point tracking (MPPT), tested on a real experimental platform.

Keywords: Water Pumping System, Conventional Components, Low Power Pumps, Maximum Power Point Tracking

1 Introduction

The use of photovoltaic energy for water pumping systems is a solution that has been widely researched and implanted [1], [2]. DC motor driven pumps are already in use in several countries, but some problems (mostly maintenance due the presence of commutator and brushes) has made researchers find other solutions [3].

One of this solutions is a water pumping system equipped with AC motors due to its advantages, mainly its ruggedness and low cost [2]. However, one problem is the fact that the market is being controlled by a few manufacturers able to afford the continuous technology development, causing low spare availability and relatively high prices for dedicated systems [4]. Hence, fully standard components systems becomes attractive [4], [5].

Dedicated PV water pumping systems are formed typically by a power converter, DC motor and PV string for power generation. Low power PV water pumping systems based on standard AC motors are not usual, because a higher voltage is needed to power the motor, which requires a string with a large number of PV modules. Standard Frequency Converters (SFCs) and AC motors are extensively used in industrial applications and they have been seldom used in PV

water pumping systems [4], [5]. The main advantages of this approach in comparison to dedicated systems includes manufacturers' independence and better component availability, lower cost because the components are manufactured in large quantities and increased reliability of the system because they are designed to work in industrial environment [5].

SFCs are produced for AC fixed input voltage from the grid (single or three-phase) and, therefore, needs a minimum voltage level on its DC-link for proper operation. One initial problem is the fact that a large number of PV modules are needed to reach this minimum operating voltage. For low power systems, where the power of the motor is below 1,5 kW, this large number of PV modules implies a high value of surplus power installed. On the other hand, the number of necessary PV modules to generate the power of the pump needed implies a undervoltage value to operate the SFC. Another problem, listed by Ramos et al. (2010), is the lack of maximum power point tracking (MPPT). This paper presents an approach with a DC/DC converter as a solution of these two problems, a step-up with MPPT is implemented using a with experimental testing on a real platform.

2 Photovoltaic Water Pumping System

As demonstrated by Abella et al. 2003, a PV array can be directly connected to a SFC to drive an AC pump. The SFC needs a minimum DC-link voltage level to operate in normal conditions. This value varies depending on the type of converter (single-phase or three-phase). For the single-phase SFC ACS355, these values are shown on Table 1. The DC values refer, approximately, to the peak value of the AC voltage. These values are for rated power. For lower power (lower radiation) and consequently lower speeds, the DC voltage can also be lower, because of scalar control. The system proposed is shown on Figure 1.

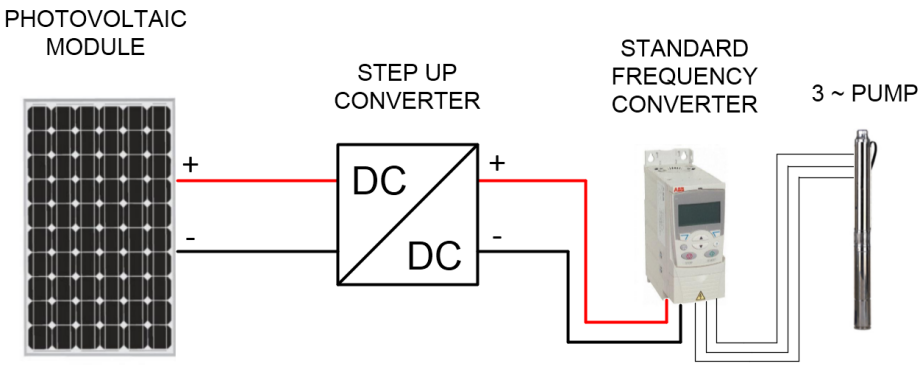

Fig. 1. Configuration of proposed PV water pumping system.

Table 1: Single-phase SFC ACS355.

AC Supply voltage [Min-Max]	200 - 240 V
DC-link voltage (on DC Bus) [Min-Max]	280 - 340 V

For proper functioning, the DC-link voltage obtained from the PV string must attend the minimum value of the SFC and the input voltage must be close to the maximum power voltage of the PV string [5]. To attend the power at the DC-link of the SFC, a DC/DC step-up converter which rises the voltage level at the output is the proposed solution in this paper. The step-up converter is controlled by a Proportional-Integrative (PI) controller which generates the Pulse-Width Modulation (PWM) pulses. The reference voltage (V_{ref}) is defined by a MPPT algorithm as described later.

For the SFC operation, the so-called PID Macro is utilized for control. This macro, which is a pre-parametrized list of parameters, is available by the manufacturers for closed-loop process control. In this application, the process variable is the DC-link voltage. So, the SFC imposes the DC voltage according to an external reference value (set-point). This reference is set to 300 V. This means that the SFC works with a fixed DC-link voltage and the reference voltage of the PV string is imposed by the step-up converter according to the MPPT algorithm.

To operate in this way, the SFC requires configuration of a set of parameters, such as the operation method that will be used, analog and digital input and output terminals, acceleration and deceleration times, and principally the PID parameters: Proportional Gain (K_p), integral time (T_i) and derivative time (T_d) [5].

2.1 Maximum Power Point Tracking

A general issue in PV generation is the tracking the maximum power available at the PV string output. The need of an algorithm to track the Maximum Power Point (MPP) comes from the non-linearity of the I-V curve of a PV module. The MPPT technique consists in adjusting the output voltage of the PV string to extract the maximum power independently of any changes in the irradiation or temperature.

In this work, the MPPT method implemented was the P&O algorithm, due to its simplicity and low computational resources [6]. P&O is the most common method of MPPT algorithms, since it is widely used in the control of the power converters in PV applications and does not require any information about the PV modules characteristics to perform the maximum power point tracking [8].

Basically, the P&O algorithm perturbs the voltage and analyses the change on the power value. These perturbations on the voltage are successive steps on the operation point that creates a change in power. If this change is positive, the perturbations are applied on the same direction, otherwise the perturbations are applied on the opposite direction. The steps followed by the algorithm are illustrated on the flow chart of the Figure 2 with the variables defined in the Table 2.

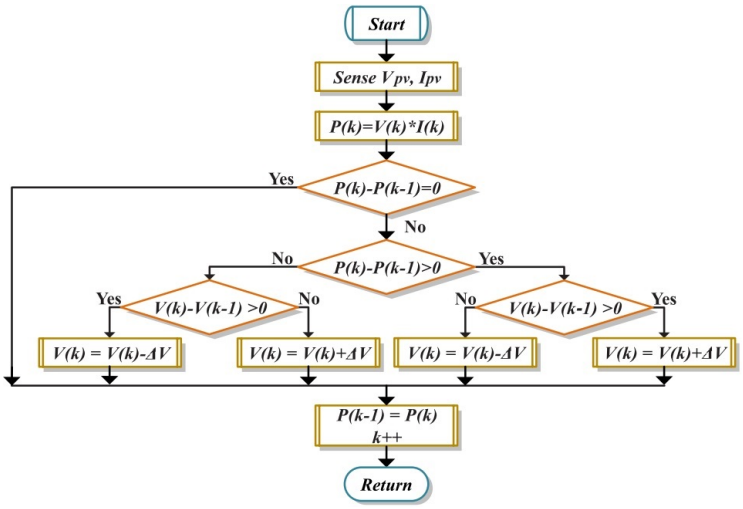

Fig. 2. State flow chart of P&O MPPT algorithm [6].

Table 2: Description of variables presented in flow chart of Figure 2 [6].

Variable	**Description**
V_{pv}	Voltage measured from the PV Panel
I_{pv}	Current measured from the PV Panel
$D(k)$	Duty cycle in present iteration
$D(k-1)$	Duty cycle in past iteration
$P(k)$, $V(k)$, $I(k)$	Power, Voltage and Current in present iteration
$P(k-1)$, $V(k-1)$, $I(k-1)$	Power, Voltage and Current in past iteration
ΔV and ΔI	Voltage increment and Current Increment
$k++$	Change for next iteration

The MPPT algorithm generates the reference voltage value (V_{ref}) for the step-up converter. This value is the reference for the PI controller, which reads the actual voltage value of V_{pv}, the reference voltage (given by MPPT algorithm) and generates the pulses of the duty-cycle for the switch of the step-up.

3 Proposed Solution

As an approach to solve the problems referred in previous section, a DC/DC step-up converter is applied to implement the MPPT and operate the PV string with a large range of voltages.

DC/DC converters are power electronic circuits for power processing that convert a DC voltage value to another level, higher or lower, depending on the

converter. There are a lot of types of converters, and they are used in large scale in many areas, like UPS, electrical drives, renewable systems, DC motor control systems and so on [7]. The step-up converter, or booster converter, is a switching circuit that elevates the value of the input voltage to the output. The electrical scheme of this type of converter is shown on Figure 3.

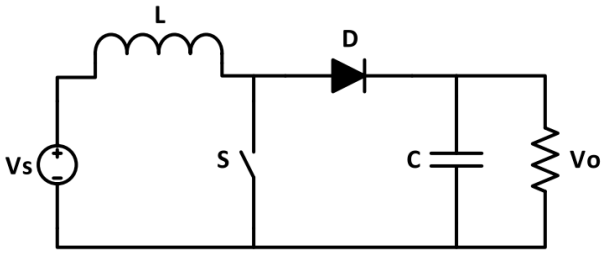

Fig. 3. Step-up converter.

The electric scheme of the proposed system is shown in Figure 4. The step-up is installed between the PV string and the DC-link of the SFC. It is composed by an inductor, a diode and a power switch (IGBT). The block diagram of step-up control with MPPT implemented is shown on Figure 5.

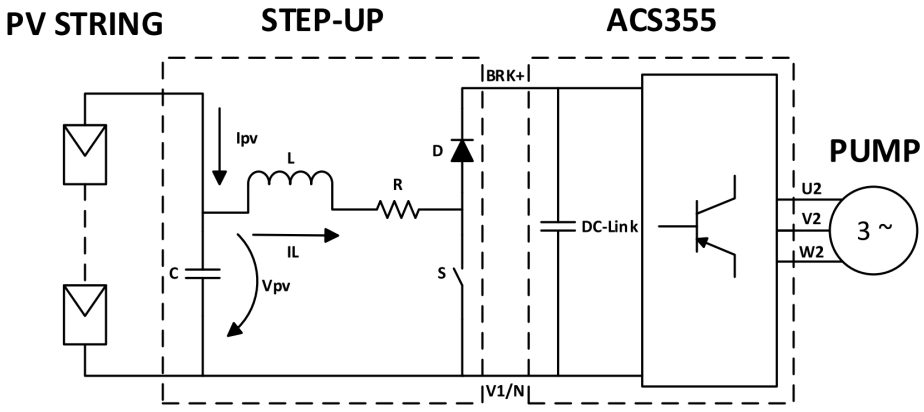

Fig. 4. Proposed PV water pumpin system.

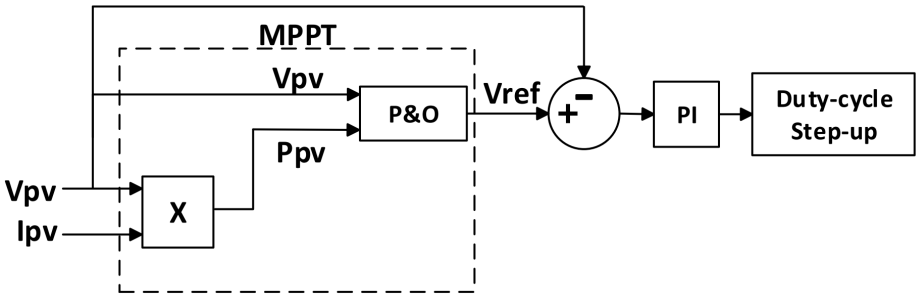

Fig. 5. Step-up control with MPPT.

One challenge is the adjust of the dynamics between the two power stages: the step-up converter and the SFC. The step-up performs the MPPT algorithm with a determined frequency, and the PID macro of the SFC adjusts the speed of the pump to maintain the voltage on the DC-link equal to reference (V_{SP}).

Hence, the PID macro parameter's K_p and T_i, acceleration and deceleration time of the SFC, must be adjusted to match the dynamics between these two power stages. According to the tests achieved on the experimental platform, the values of these parameters used in this work are show on Table 3.

Table 3: Components of the system.

Parameter	**Value**
Step-up PI Controller	$K_p = 500\text{x}10^{-6}$; $K_i = 0{,}10$
SFC PID Controller	$K_p = 0{,}2$; $T_i = 2$ s; $T_d = 0$
SFC Acceleration time	0.1 s
SFC Deceleration time	0.1 s

3.1 Experimental Platform

To evaluate the functioning and performance of the system proposed in this work, a solar photovoltaic water pumping system at the Polytechnic Institute of Bragança has been used. The system is composed by the elements described on Table 4.

Table 4: Components of the system.

Component	**Equipment Used**
Pump	Termar B20 3∼ 1.5 kW - 2 HP Submersible
Standard Frequency Converter	ABB ACS355-01E-07A5-2
Step-up Power Switch and Diode	Two IGBTs of Mitsubishi PM75RLA120
Step-up Inductor	Mundorf BT140 12 mH/0,45 Ohm
Photovoltaic Modules	Fluitecnik's FTS-220P

The experimental platform components utilized in this work are shown on Figure 6. The PV modules are installed on the roof of the laboratory. The step-up was implemented in Simulink and the real time control was performed using the 1103 controller board from dSPACE.

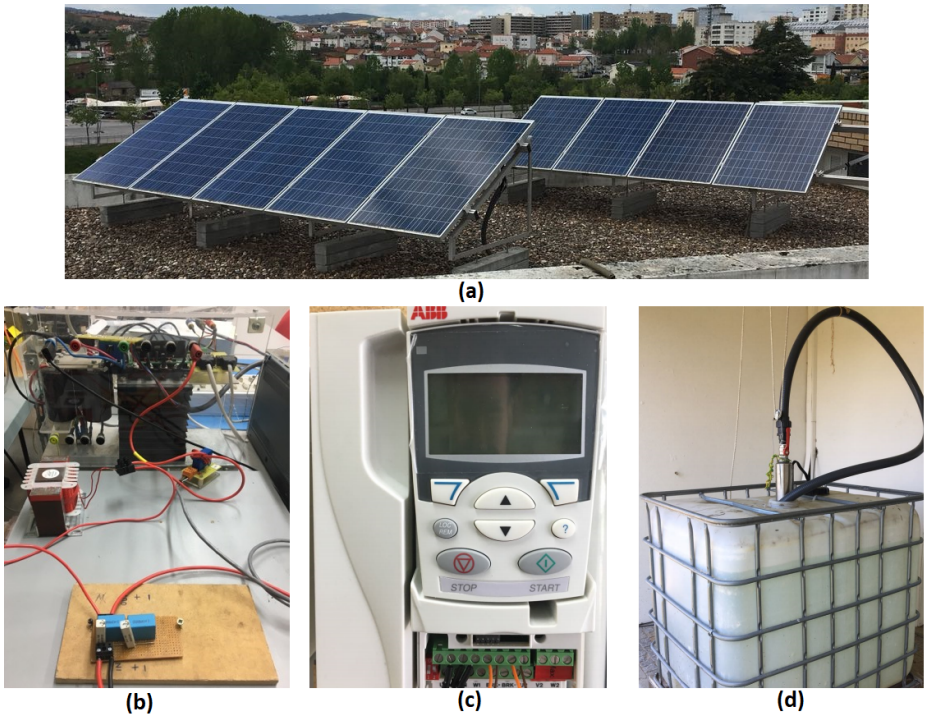

Fig. 6. Experimental platform, (a) PV string, (b) step-up converter, (c) single-phase ACS355, (d) water tank and pump.

The experimental results were carried out with 4, 6 and 8 PV modules available on the roof of the laboratory. All tests were performed under same solar radiation and temperature levels, acquired by the measuring system present on the laboratory. These values are shown on Table 5.

Table 5: Comparison of the power and voltage of each set.

Condition	**Value**
Date and Time	07/05/2018 - 11:00
Radiation level	G = 810 W/m^2
Ambient Temperature	T_a = 28°C
PV Module Temperature	T_{pv} = 45°C

4 Practical Implementation of the System and Evaluation of the Results

Figures 7, 8 and 9 show the V_{pv}, V_{dc}, I_{pv} and P_{pv} curves for 4, 6 and 8 PV modules, respectively. V_{SP} is set 300 V and the MPPT is running two times per second with voltage increment of 1 V.

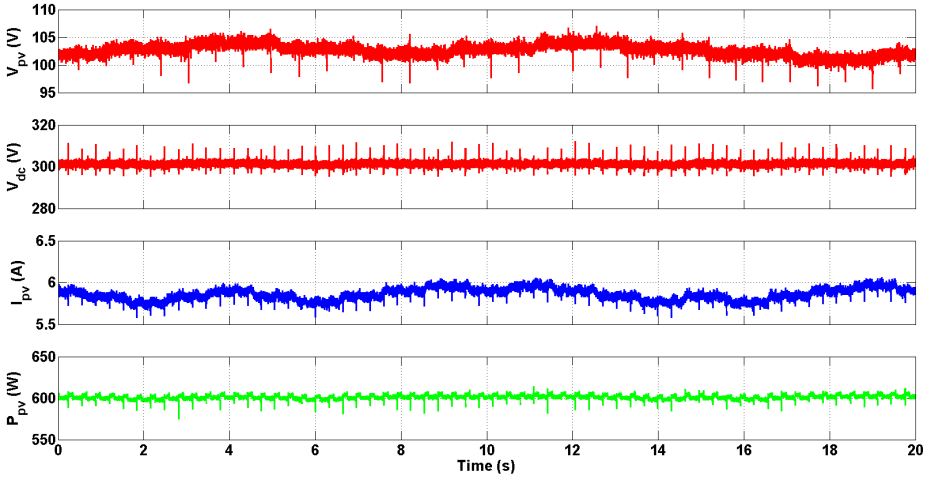

Fig. 7. V_{pv}, V_{dc}, I_{pv} and P_{pv} for 4 PV modules.

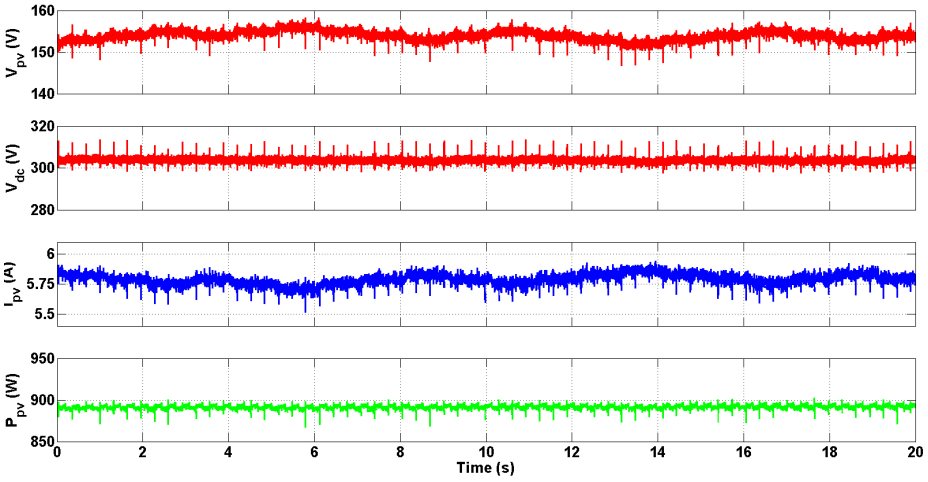

Fig. 8. V_{pv}, V_{dc}, I_{pv} and P_{pv} for 6 PV modules.

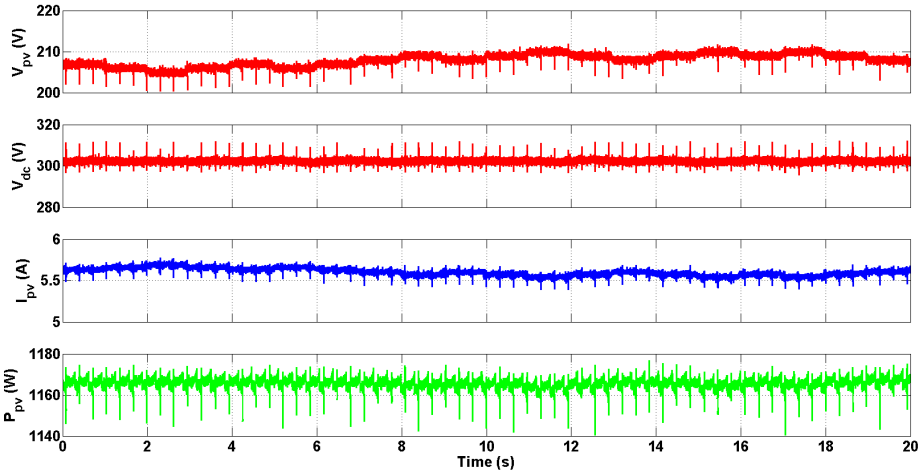

Fig. 9. V_{pv}, V_{dc}, I_{pv} and P_{pv} for 8 PV modules.

For all conditions V_{dc} is 300 V and V_{pv} varies according to the MPPT algorithm, validating the parameters of PID controller of the SFC and the match the dynamics between these two power stages. The PV power curve as well as the water pump operation show the expected results, showing that the step-up controls the PV string voltage using the MPPT algorithm applying successive steps in order to operate in MPP. The SFC PID macro controls the DC-link voltage indirectly by adjusting the speed of the motor.

These results show that the step-up allows the driving of low power pumps (up to 1,5 kW) using only the necessary number of PV modules. For comparison, Table 6 shows the power and voltage (in MPP) provided by each set of PV modules tested.

Table 6: Comparison of the power and voltage of each set.

Size of PV string	**Power and Voltage**
4 PV modules	P = 880 W and V_{pv} = 117 V
6 PV modules	P = 1320 W and V_{pv} = 176 V
8 PV modules	P = 1760 W and V_{pv} = 235 V

This values shown on Table 6 shows that for 8 PV modules, the power is greater than the 1,5 kW (beyond the necessary) and the voltage level is less than 280 V (shown on Table 1) for rated operation, and Figure 9 shows V_{pv} variating between 200 V - 210 V and V_{dc} fixed at 300 V for rated operation of the SFC, validating the solution proposed.

5 Conclusions

SFCs can be used in PV pumping applications. This alternative offers significant advantages compared with those based on PV dedicated controller and pumps. Indeed, SFCs are widely available all over the world and their price is significantly lower than those of PV dedicated power inverters. To solve the problem of the number of PV modules on low power systems and the implementation of a MPPT, the addition of a DC/DC converter has been proven to operate as expected. The validity of these proposals has been evaluated experimentally in a real system.

6 Acknowledgements

The authors wish to thank Polytechnic Institute of Bragança, JG Electrical Installations and the Research Center in Digitalization and Intelligent Robotics (CeDRI), for the experimental set-up available.

References

1. Rohit, K. B., Karve, G. M., Khatri: "Solar Water Pumping System", International Journal of Emerging Technology and Advanced Engineering, Volume 3, Issue 7, July, 2013.
2. Miladi, M., Abdelghani-Bennani, A. B., Slama-Belkhodja, I., M'Saad, H.: "Improved low cost induction motor control for stand alone solar pumping," 2014 International Conference on Electrical Sciences and Technologies in Maghreb (CISTEM), Tunis, 2014, pp. 1-8.
3. Malla, S. G., Bhende, C. N., Mishra, S.: "Photovoltaic based water pumping system," 2011 International Conference on Energy, Automation and Signal, Bhubaneswar, Odisha, 2011, pp. 1-4.
4. Abella, M. A., Lorenzo, E., Chenlo, F.: "PV Water Pumping Systems based on standard frequency converters", Progress in Photovoltaics Research and Applications 11, 179-191.
5. Fernández-Ramos, J., Narvarte-Fernández, L., Poza-Saura, F.: "Improvement of photovoltaic pumping systems based on standard frequency converters by means of programmable logic controllers", Solar Energy, Volume 84, Issue 1, 2010.
6. Zamora, A. C., Vazquez, G., Sosa, J. M., Martinez-Rodriguez, P. R., Juarez, M. A.: Eciency based comparative analysis of selected classical mppt methods, in 2017 IEEE International Autumn Meeting on Power, Electronics and Computing (ROPEC), Nov. 2017, pp. 16.
7. Hart, D. W.: Introduction to power electronics, Prentice Hall, 1997.
8. Jiang, J. A., Su, Y. L., Kuo, K. C., Wang, C. H., Liao, M. S., Wang, J. C., Huang, C. K., Chou, C. K., Lee, C. H., Shieh, J. C.: On a hybrid mppt control scheme to improve energy harvesting performance of traditional two-stage inverters used in photovoltaic systems, Renewable and Sustainable Energy Reviews, vol. 69, pp. 1113 1128, 2017.
9. Narvarte, L. , Poza, F., Lorenzo, E.: "Specification and testing of PV pumps for a Moroccan project". Prog. Photovolt: Res. Appl., 14: 733-741, 2006.